A Generalized Class of Fractal-Wavelet Transforms for Image Representation and Compression

Edward R. Vrscay
Department of Applied Mathematics
Faculty of Mathematics
University of Waterloo
Waterloo, Ontario, Canada N2L 3G1
e-mail: ervrscay@links.uwaterloo.ca

Abstract

The action of an affine Fractal Transform or (Local) Iterated Function System with Grey Level Maps (IFSM) on a function $f(x)$ induces a simple mapping on its expansion coefficients c_{ij} in the Haar wavelet basis. This is the basis of the discrete *fractal-wavelet transform* where subtrees of the wavelet coefficient tree are scaled and copied to lower subtrees. Such transforms, which we shall also refer to as *IFS on wavelet coefficients* (IFSW) were introduced into image processing with other (compactly supported) wavelet basis sets in an attempt to remove the blocking artifacts that plague standard IFS block-encoding algorithms.

In this paper a set of generalized 2D fractal-wavelet transforms is introduced. Their primary difference from usual IFSW transforms lies in treating "horizontal", "vertical" and "diagonal" quadtrees independently. This may seem expensive in terms of coding. However, the added flexibility provided by this method, resulting in a marked improvement in accuracy and low degradation with respect to quantization, makes it quite tractable for image compression.

As in the one-dimensional case, the IFSW transforms are equivalent to recurrent IFSM with condensation functions. The net result of an affine IFSW is an extrapolation of high frequency wavelet coefficients which grow or decay geometrically, according to the magnitudes of fractal scaling parameters α_{ij}. This provides a connection between the α_{ij} and the regularity/irregularity properties of regions of the image. IFSW extrapolation also makes possible "fractal zooming." The results of computations, including some simple compression methods, are also presented.

AMS Subject Classifications: 41A, 41A35, 46E30, 65D15, 68U10
Key words: Iterated function systems, fractal transforms, fractal-wavelet transforms, image compression, inverse problems

To appear in the January 1998 issue of the *Canadian Journal of Electrical and Computer Engineering* on "Visual Computing and Communications" (S. Panchanathan, Guest Editor).

1 Introduction

The purpose of this paper is to introduce and analyze a general class of affine two-dimensional discrete fractal-wavelet transforms primarily for use in fractal image compression. The standard fractal-wavelet transforms discovered independently by a number of workers (for example, [8, 9, 15, 19, 33, 34]) involve a scaling/copying of wavelet coefficient subtrees to lower subtrees, quite analogous to the geometrical action of Iterated Function Systems (IFS) [2, 1, 17] on sets or the action of Fractal Transforms [4] and Iterated Function Systems with Grey-Level Maps (IFSM) [14] on functions.

In the case of Haar wavelets, there is an obvious connection between the scaling/copying of wavelet subtrees and the contraction and translation of the function (or a portion of it) by an IFSM. Indeed, this inspired people to define the same types of block transformations on coefficients of generalized (non-Haar) wavelets with compact support. A detailed study of the one-dimensional case [26] has shown, however, that the relation to IFSM is not straightforward. In general, fractal-wavelet transforms are equivalent to recurrent, local IFSM with condensation functions. Herein lies one advantage of fractal-wavelet methods over the standard fractal (IFSM) transform applied to image functions: The action of local geometrical IFSM maps on subsets of the image function in pixel space ($[0,1]^2$) is translated into IFSM-type operations over orthogonal components of the image function which may or may not be mixed together. With fractal-wavelet transforms, the convenience of orthogonality is automatically available, which is not the case when standard fractal transforms are used [30, 35].

The relationship between fractal-wavelet transforms, which we shall also refer to as *IFS on wavelet coefficients* (IFSW), and IFSM is even more complicated in the two-dimensional case due to the existence of more than one principal set of wavelet coefficient quadtrees. In this paper, 2D fractal-wavelet transforms are applied to the standard tensor-product wavelet basis composed of "horizontal", "vertical" and "diagonal" subspaces. These transforms operate on the three subspaces independently, a deviation from the normal fractal-wavelet transform/IFSM case. Such an IFSW allows a fractal-based method to be applied to orthogonal subspaces of a function, either independently or dependently. At first glance, such a generalization may seem expensive in terms of image compression (for example, more scaling factors and possibly parent block codes). However, the flexibility afforded by the method is an advantage. The marked improvement in accuracy as well as good tolerance with respect to the quantization of the scaling factors compensate for this expense.

The strength of the fractal-wavelet transform in image representation and compression lies in its ability (and hitherto unexplored possibilities) to combine the best of two worlds: (1) *fractal transforms* with their inherent properties of scaling and (local) self-similarity and (2) *wavelets* with the power of multiresolution analysis and the fast wavelet transform. The use of wavelet methods may also permit the incorporation of known properties of vision [13, 40] into coding schemes.

The structure of this paper is as follows. For the benefit of the general reader, the remainder of this section is devoted to the basic ideas of Iterated Function Systems and IFSM. Some illustrative examples are presented in Appendix A. In Section 2, the fractal-wavelet transform for one-dimension (functions on $X \subset \mathbf{R}$) is introduced along with some examples. Two-dimensional fractal-wavelet transforms are introduced in Section 3 with some examples. The inverse problem of image approximation using the 2D fractal-wavelet transforms is discussed in Section 4 along with an outline of its mathematical setting. In Section 5 the generalized 2D fractal-wavelet transform is applied to images. Some rather

elementary compression methods using simple quantization are explored in order to give an idea of the effectiveness of the method. In Section 6 we explore the fact that the fractal-wavelet transform uses high frequency information to extrapolate low frequency parent block wavelet coefficients. From the known behaviour of wavelet transforms at regular and irregular points of an image, the behaviour of the affine IFSW coefficients α_{ij} can be used to characterize edges or smooth regions. The extrapolation can also be exploited to perform a "fractal zooming" of the image. Some concluding remarks are made in Section 7.

1.1 Iterated Function Systems on Function Spaces

"Iterated Function Systems" (IFS) is the name introduced by Barnsley and Demko [2] to denote a system of contraction mappings on a complete metric space. The idea was independently developed earlier by Hutchinson [17] who showed how typically self-similar fractal sets and measures could be generated by a parallel action of such systems of contraction mappings. The IFS maps plus a set of associated probabilities (IFSP) define operators which act on probability measures. As a result, early IFS research work focussed on the representation of images by measures and their approximation by IFSP invariant measures. However, since it is more convenient to represent images and signals by functions, the goal of IFS-type methods became the approximation of images and signals by functions which are generated by the iteration of an IFS-type operator.

Iterated Function Systems with Grey Level Maps (IFSM) are an example of an IFS or *fractal transform* method over an appropriate space of functions $\mathcal{F}(X)$ which represent our images or signals. (A more detailed mathematical treatment of IFSM is given in [14, 15].) Here (X, d) denotes a compact metric space, the "base space" or "pixel space" of support for the signals and images, typically $[0,1]$ or $[0,1]^2$ with Euclidean metric. In this study, without loss of generality, the space of functions $\mathcal{F}(X)$ will be $\mathcal{L}^2(X)$, the set of functions $f : X \to \mathbf{R}$ such that $\| f \|_2^2 = \int_X |f(x)|^2 dx < \infty$.

An N-map IFSM is defined by:

1. **The IFS component:** $\mathbf{w} = \{w_1, w_2, \ldots, w_N\}$ where each $w_i : X \to X$ is a contraction, i.e. there exists a $c_i \in [0,1)$ such that $d(w_i(x), w_i(y)) \leq c_i d(x,y)$ for all $x, y \in X$. For convenience, affine IFS maps are primarily used in applications.

2. **The grey level component:** $\Phi = \{\phi_1, \phi_2, \ldots, \phi_N\}$ where each $\phi_i : \mathbf{R} \to \mathbf{R}$ is Lipschitz, i.e. there exists a $K_i \geq 0$ such that $|\phi_i(t_1) - \phi_i(t_2)| \leq K_i |t_1 - t_2|$ for all $t_1, t_2 \in \mathbf{R}$. Affine grey-level maps of the form $\phi_i(t) = \alpha_i t + \beta_i$, $\alpha_i, \beta_i \in \mathbf{R}$ are typically employed.

Associated with an IFSM $(\mathbf{w}, \Phi)$ is a *fractal transform* operator $T : \mathcal{F}(X) \to \mathcal{F}(X)$ with the following action. For each $x \in X$ define its N *fractal components* f_i as:

$$f_i(x) = \begin{cases} \phi_i(u(w_i^{-1}(x))), & x \in w_i(X), \\ 0, & x \notin w_i(X). \end{cases} \tag{1}$$

(One can also an additional condition that for each $x \in X$ there exists at least one "preimage" $w_{i^*}^{-1}(x)$, but this is not necessary.) Now, given a $u \in \mathcal{F}(X)$, its image Tu will be defined as follows:

$$(Tu)(x) = \sum_{i=1}^{N} f_i(x). \tag{2}$$

Geometrically, the action of the operator T may be viewed in terms of its action on the graph of u. Each term $u(w_i^{-1}(x))$ represents a shrunken copy of the graph of u which is supported on the set $w_i(X)$. The grey level map ϕ_i then distorts this shrunken copy in the grey level direction to produce the fractal component f_i. The fractal transform adds up these fractal components to produce $(Tu)(x)$.

Example: The two-map IFSM on $X = [0, 1]$:

$$\begin{aligned} w_1(x) &= 0.6x, & \phi_1(t) &= 0.5t + 0.2, \\ w_2(x) &= 0.6x + 0.4, & \phi_2(t) &= 0.5t + 0.5. \end{aligned} \tag{3}$$

The action of the associated fractal transform operator T on the function $u(x) = 4x(1-x)$ is shown in Figure 1(a). There are two fractal component functions, $f_1(x)$ and $f_2(x)$, which are supported on the subsets $w_1(X) = [0, 0.6]$ and $w_2(X) = [0.4, 1]$, respectively. All points $x \in w_1(X) \cap w_2(X) = [0.4, 0.6]$, have both fractal components which must be then added to produce $(Tu)(x)$. For points $x \in [0, 0.4)$ and $x \in (0.6, 1]$, the function value $(Tu)(x)$ is determined by only one fractal component, namely, $f_1(x)$ for the former and $f_2(x)$ for the latter.

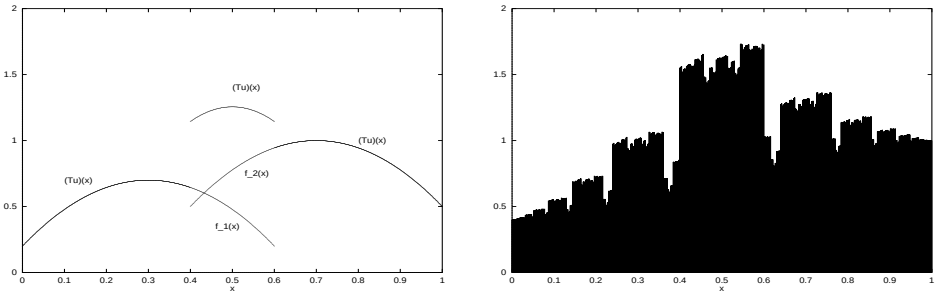

Figure 1: (a) Graph of $(Tu)(x)$ where $u(x) = 4x(1-x)$ and T is the contractive operator for the two-map IFSM given in Eq. (3). (b) The fixed point attractor function $\bar{u}(x) = T\bar{u}(x)$.

Under suitable conditions on the w_i and the ϕ_i involving their Lipschitz factors, the IFSM operator T is contractive in $\mathcal{F}(X)$. From Banach's Fixed Point Theorem, there exists a unique fixed point $\bar{u} = T\bar{u}$ (see [14]). The IFSM operator in the above example is contractive in $\mathcal{L}^2([0, 1])$. A histogram approximation of its fixed point function $\bar{u}$ is shown in Figure 1(b). (This approximation was obtained by repeated application of T on a function, as begun in Figure 1(a), until satisfactory convergence was achieved.) From the property $\bar{u} = T\bar{u}$, the graph of $\bar{u}$ is a union of two shrunken and modified copies of itself. In most applications in the literature the sets $w_i(X)$ have minimal overlap, i.e. at a finite number of points on X. (In fact, such overlap is ignorable in the $\mathcal{L}^2$ sense.)

The IFSM method may be generalized to "place-dependent" IFSM (PDIFSM) with grey level maps $\phi_k : \mathbf{R} \times X \to \mathbf{R}$. In other words, the ϕ_k depend on both the grey level value at a preimage as well as the location of the preimage itself. (This is analogous to IFS with place-dependent probabilities [3].) This is the basis of the "Bath Fractal Transform" (BFT) [27, 28] which has been quite effective in coding images. An example of this transform is given in Appendix A. The action of the BFT resembles that of certain fractal-wavelet transforms that will be defined below.

It is extremely advantageous to consider a further generalization, namely the *local* IFSM [4] with IFS maps w_{ij} that map *subsets* $I_j \subset X$ to smaller subsets $J_k \subset X$. This is the basis of fractal block encoding first described by Jacquin [18]. The associated local IFSM

operator maps modified copies of the signal/image on the I_j onto the J_k. It would seem more reasonable to expect that signals and images may be approximated as unions of local copies of themselves, as opposed to copies of the entire signal. In fact, most fractal image compression methods are still based on this type of block encoding. An example is given in Appendix A.

An IFSM operator of special significance is the following:

$$T(f)(x) = \theta(x) + \sum_i \alpha_i f(w_i^{-1}(x)). \tag{4}$$

Here, the function $\theta(x)$ acts as a "condensation" function for the IFSM. These operators will be relevant in our study of fractal-wavelet transforms.

The essence of fractal image compression - indeed, IFS-type methods in general, including the fractal-wavelet transforms in this paper - is the following:

> Given a "target" image $v \in \mathcal{F}(X)$ which we seek to approximate or "compress" to a desirable accuracy $\epsilon > 0$, find an IFSM $(\mathbf{w}, \Phi)$ with associated (contractive) fractal transform operator T such that $\| v - \bar{u} \|_2^2 < \epsilon$, where $\bar{u} = T\bar{u}$ is the fixed point of T.

The theoretical aspects of this inverse problem are discussed in [15]. Practical aspects of fractal image compression are dealt with in [11, 12]. The recent book by Lu [21] is an excellent and comprehensive treatment of the subject.

Finally, the basis of the fractal-wavelet transform lies in the following property. Let $\{q_i(x)\}$ be an orthonormal basis of $\mathcal{L}^2(X)$. Then for each $f \in \mathcal{L}^2(X)$ there exists a unique sequence $\mathbf{c} \in l^2(\mathbf{N})$ of expansion coefficients $c_i = \langle f, q_i \rangle$. Given an IFSM operator $T : \mathcal{L}^2(X) \to \mathcal{L}^2(X)$ there exists a corresponding operator $M : l^2(\mathbf{N}) \to l^2(\mathbf{N})$. The following figure illustrates this feature:

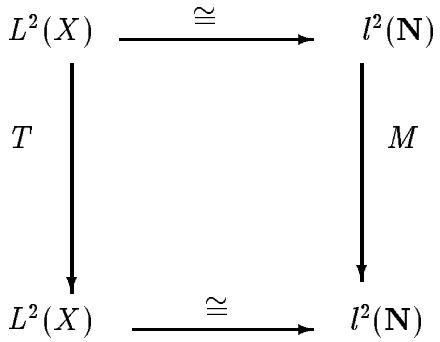

If the IFSM operator T is affine or linear, then the operator M will also be affine or linear. If T is contractive in $\mathcal{L}^2(X)$, then M is contractive in $l^2(\mathbf{N})$. (See [15] for further discussion.) When the orthonormal basis is the Haar wavelet basis $\{\psi_{ij}\}$, then the operator M becomes a mapping of wavelet coefficient subtrees to lower subtrees. Such mappings will be introduced in the next section.

2 Fractal-Wavelet Transforms in One Dimension

2.1 The Wavelet Expansions Considered

We briefly review the one-dimensional case in order to (a) establish the notation and (b) show both the similarities as well as the differences between the one- and two-dimensional

cases. First assume a standard dyadic multiresolution approximation of $\mathcal{L}^2(\mathbf{R})$ as follows [10, 22, 39]:

1. A sequence of nested subspaces $V_k \in \mathcal{L}^2(\mathbf{R})$, $k \in \mathbf{Z}$, where $V_k \subset V_{k+1}$. (V_k contains the set of all approximations of functions $f \in \mathcal{L}^2(\mathbf{R})$ at resolution 2^k.) Moreover $\cap_n V_n = \{\emptyset\}$ and $\lim_{n\to\infty} \cup V_n = \mathcal{L}^2(\mathbf{R})$.

2. The sequence of orthogonal complements $W_k \perp V_k$ such that $W_k \oplus V_k = V_{k+1}$, $k \in \mathbf{Z}$. This implies that for any $m \in \mathbf{Z}$ and $n > 0$,

$$V_m \oplus W_m \oplus W_{m+1} \oplus \ldots \oplus W_{m+n} = V_{m+n+1}. \tag{5}$$

3. A *scaling function* $\phi \in \mathcal{L}^2(\mathbf{R})$ such that the functions

$$\phi_{ij}(x) = 2^{i/2}\phi(2^i x - j), \qquad j \in \mathbf{Z}, \tag{6}$$

   form an orthonormal basis for V_i.

4. The orthogonal *(mother) wavelet* $\psi \in \mathcal{L}^2(\mathbf{R})$ such that the functions

$$\psi_{ij}(x) = 2^{i/2}\psi(2^i x - j), \qquad j \in \mathbf{Z}, \tag{7}$$

   form an orthonormal basis for W_i. It follows that the set $\{\psi_{ij}\}$, $i, j \in \mathbf{Z}$, forms a complete orthonormal basis for $\mathcal{L}^2(\mathbf{R})$.

In the case of the Haar wavelet system,

$$\phi_{00}(x) = 1, \quad x \in [0,1), \qquad \psi_{00}(x) = \begin{cases} 1, & x \in [0, \frac{1}{2}), \\ -1, & x \in [\frac{1}{2}, 1). \end{cases} \tag{8}$$

We shall be concerned with the case $m = 0$ in Eq. (5), in particular, functions $f \in \mathcal{L}^2(\mathbf{R})$ which admit wavelet expansions of the form (in the $\mathcal{L}^2(\mathbf{R})$ sense)

$$f(x) = b_{00}\phi_{00}(x) + c_{00}\psi_{00}(x) + \sum_{i=1}^{\infty}\sum_{j=0}^{2^i-1} c_{ij}\psi_{ij}(x), \tag{9}$$

where $b_{00} = \langle f, \phi_{00}\rangle$ and $c_{ij} = \langle f, \psi_{ij}\rangle$. It is also assumed that the scaling function ϕ (hence ψ) has compact support on $\mathbf{R}$. This implies that f has compact support. (In the special case of the Haar wavelets, the support of f is $[0,1]$.) The wavelet expansion coefficients are conveniently displayed in the form of an infinite tree as shown below.

<table>
<tr><td colspan="8">b_{00}</td></tr>
<tr><td colspan="8">c_{00}</td></tr>
<tr><td colspan="4">c_{10}</td><td colspan="4">c_{11}</td></tr>
<tr><td colspan="2">c_{20}</td><td colspan="2">c_{21}</td><td colspan="2">c_{22}</td><td colspan="2">c_{23}</td></tr>
<tr><td>B_{30}</td><td>B_{31}</td><td>B_{32}</td><td>B_{33}</td><td>B_{34}</td><td>B_{35}</td><td>B_{36}</td><td>B_{37}</td></tr>
</table>

Note that each entry B_{ij} represents a binary tree of infinite length. Such a tree with root c_{ij} will also be referred to as the *block* B_{ij}.

2.2 Some 1D Fractal-Wavelet Transforms

We now consider some simple IFS-type operations on the wavelet tree shown above. These are examples of discrete *fractal wavelet transforms* which shall also be referred to as *IFS on wavelet coefficients* or simply IFSW. Without loss of generality, we set $b_{00} = 0$. These and other examples are discussed in more detail in [26].

Example 1: Using the above notation, consider the following transformation:

$$M \ : \ B_{00} \ \rightarrow \ \begin{array}{|c|c|}\hline \multicolumn{2}{|c|}{c_{00}} \\ \hline \alpha_1 B_{00} & \alpha_2 B_{00} \\ \hline \end{array} \quad , \qquad |\alpha_i| < \frac{1}{\sqrt{2}}. \tag{10}$$

The blocks $\alpha_i B_{00}$ represent the binary trees obtained by multiplying every element c_{ij} of B_{00} by the constants α_i, The restrictions on the α_i follow from the condition that the wavelet coefficient sequence c_{ij} belongs to $l^2(\mathbf{N})$. Iteration of this operator is straightforward:

$$M^2(B_{00}) \ = \ \begin{array}{|c|c|c|c|}\hline \multicolumn{4}{|c|}{c_{00}} \\ \hline \multicolumn{2}{|c|}{\alpha_1 c_{00}} & \multicolumn{2}{|c|}{\alpha_2 c_{00}} \\ \hline \alpha_1^2 B_{00} & \alpha_1\alpha_2 B_{00} & \alpha_2\alpha_1 B_{00} & \alpha_2^2 B_{00} \\ \hline \end{array} \quad , \ \text{etc.} \ . \tag{11}$$

The dilatation/translation relations between wavelet basis functions allow us to construct the IFSM operator T (cf. Eq. (4)) that corresponds to the IFSW operator M. If B_{00} represents the wavelet expansion of f then, from Eq. (7),

$$(Tf)(x) = c_{00}\psi(x) + \sqrt{2}\alpha_1 f\left(w_1^{-1}(x)\right) + \sqrt{2}\alpha_2 f\left(w_2^{-1}(x)\right), \tag{12}$$

a two-map IFSM with condensation function $c_{00}\psi(x)$, where

$$w_1(x) = \frac{1}{2}, \qquad w_2(x) = \frac{1}{2}x + \frac{1}{2}. \tag{13}$$

Note that the IFSM operator depends on the particular wavelet basis chosen.

In the special case of Haar wavelets, the mother wavelet $\psi(x)$ decomposes into nonoverlapping components:

$$\psi(x) = I_{[0,1/2)}(x) - I_{[1/2,1)}(x). \tag{14}$$

As a result the IFSM operator T can also be expressed as a simple two-map IFSM with affine grey-level maps

$$\phi_1(t) = \sqrt{2}\alpha_1 t + 1, \qquad \phi_2(t) = \sqrt{2}\alpha_2 t - 1. \tag{15}$$

If T is contractive, then its fixed point attractor function $\bar{u}$ has [0,1] as support.

However, in the case of other compactly supported wavelets, no such simple spatial decomposition into separate grey-level maps is possible. As well, the support of the attractor function $\bar{u}$ is necessarily larger than [0,1]. To illustrate, consider the particular IFSW in which $\alpha_1 = 0.4$ and $\alpha_2 = 0.6$. The IFSM operator T in Eq. (12) is contractive. Figures 2(a) and 2(b) show the IFSM attractor functions for, respectively, the Haar wavelet and "Coifman-6" cases. In both cases, we have chosen $b_{00} = 0$ and $c_{00} = 1$.

Example 2: Consider the fractal wavelet transform with four block maps as follows:

$$W_1 : B_{10} \rightarrow B_{20}, \quad W_2 : B_{11} \rightarrow B_{21}, \quad W_3 : B_{10} \rightarrow B_{22}, \quad W_4 : B_{11} \rightarrow B_{23}, \tag{16}$$

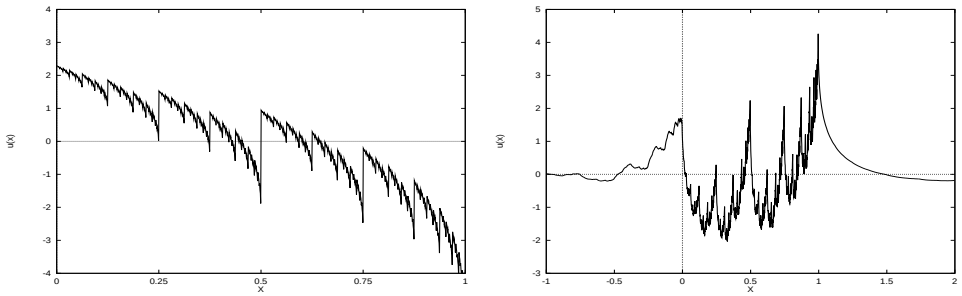

Figure 2. Attractor functions $\bar{u}$ for Example 1: (a) Haar wavelet basis, (b) (nonperiodic) Coifman-6 wavelet basis.

with associated multipliers α_i, $1 \le i \le 4$. Diagramatically,

$$M \ : \ B_{00} \ \rightarrow \ \begin{array}{|c|c|c|c|} \hline \multicolumn{4}{|c|}{c_{00}} \\ \hline \multicolumn{2}{|c|}{c_{10}} & \multicolumn{2}{c|}{c_{11}} \\ \hline \alpha_1 B_{10} & \alpha_2 B_{11} & \alpha_3 B_{10} & \alpha_4 B_{11} \\ \hline \end{array} \ . \tag{17}$$

Now iterate this process, assuming it converges to a limit $\bar{B}_{00}$ which represents the wavelet expansion of a function $\bar{u}$. Then

$$\bar{u} = c_{00}\psi_{00} \ + \ \bar{v}. \tag{18}$$

We need only focus on the function $\bar{v}$ which admits the wavelet expansion

$$\begin{array}{|c|c|c|c|} \hline \multicolumn{2}{|c|}{c_{10}} & \multicolumn{2}{c|}{c_{11}} \\ \hline \alpha_1 \bar{B}_{10} & \alpha_2 \bar{B}_{11} & \alpha_3 \bar{B}_{10} & \alpha_4 \bar{B}_{11} \\ \hline \end{array} \ . \tag{19}$$

Since $\langle \psi_{10}, \psi_{11} \rangle = 0$, etc., we may write

$$\bar{v} \ = \ \bar{v}_1 \ + \ \bar{v}_2 \ , \tag{20}$$

where the orthogonal components $\bar{v}_i$ satisfy the relations

$$\begin{aligned} \bar{v}_1(x) \ &= \ c_{10}\psi_{10}(x) \ + \ \alpha_1\sqrt{2}\bar{v}_1(2x) \ + \ \alpha_2\sqrt{2}\bar{v}_2(2x) \\ \bar{v}_2(x) \ &= \ c_{11}\psi_{11}(x) \ + \ \alpha_3\sqrt{2}\bar{v}_1(2x-1) \ + \ \alpha_4\sqrt{2}\bar{v}_2(2x-1). \end{aligned} \tag{21}$$

This "vector IFSM" is, in fact, a recurrent IFSM (with condensation functions) on $B_{00} = B_{10} \oplus B_{11}$ which "mixes" the orthogonal components B_{10} and B_{11}.

The above equations may be written in the more compact form

$$\bar{v}_i(x) \ = \ b_i(x) \ + \ \sum_{j=1}^{2} \phi_{ij}(\bar{v}_j(w_{ij}^{-1}(x))), \quad i = 1, 2, \tag{22}$$

where

$$w_{11}(x) \ = \ w_{12}(x) \ = \ \frac{1}{2}x, \ \ w_{21}(x) \ = \ w_{22}(x) \ = \ \frac{1}{2}x \ + \ \frac{1}{2}, \tag{23}$$

$$b_1(x) = c_{10}\psi_{10}(x), \ \ b_2(x) = c_{11}\psi_{11}(x) \ , \tag{24}$$

and

$$\phi_{11}(t) = \alpha_1\sqrt{2}t, \ \ \phi_{12}(t) = \alpha_2\sqrt{2}t, \ \ \phi_{21}(t) = \alpha_3\sqrt{2}t, \ \ \phi_{22}(t) = \alpha_4\sqrt{2}t \ . \tag{25}$$

Note that the contractive IFS maps w_{ij} are mappings from the *entire* base space X into itself. Even though the IFSW operator M had the appearance of a "local" transform in the

wavelet coefficient space, the equivalent IFSM is *not*, in general, a "local" IFSM. (In the special case of nonoverlapping Haar wavelets, the IFSM may be written as a local IFSM.) *The "locality" of the block transform has been passed on to the orthogonal components* $\bar{v}_1$ *and* $\bar{v}_2$ *of the function* $\bar{v}$.

Fractal-wavelet transforms of the above form may also be applied to coefficient trees in the basis of *periodized wavelets*. However, the connection to IFSM is even more complicated [26] and will not be discussed here. For the benefit of the general reader, the important properties of periodized wavelets are outlined in Appendix B along with some examples. The IFSW method is applicable to biorthogonal wavelets and other schemes employed in image analysis.

3 Fractal-Wavelet Transforms in Two Dimensions

The following subsection is primarily concerned with the notation employed for the standard tensor-product wavelet basis in $\mathbf{R}^2$.

3.1 The Wavelet Expansions Considered

We consider the standard construction of orthonormal wavelet bases in $\mathcal{L}^2(\mathbf{R}^2)$ using suitable tensor products of subspaces V_i and W_j in $\mathcal{L}^2(\mathbf{R})$ as discussed in [10, 22]. Define the sequence of nested subspaces $\mathbf{V}_k \in \mathcal{L}^2(\mathbf{R}^2)$, $k \in \mathbf{Z}$, where $\mathbf{V}_k \subset \mathbf{V}_{k+1}$ so that $\cap_n \mathbf{V}_n = \{\emptyset\}$ and $\lim_{n\to\infty} \cup \mathbf{V}_n = \mathcal{L}^2(\mathbf{R}^2)$. For each $\mathbf{V}_k$ define its orthogonal complement $\mathbf{W}_k$ so that $\mathbf{V}_{k+1} = \mathbf{V}_k \oplus \mathbf{W}_k$. For any $m \in \mathbf{Z}$ and $n > 0$,

$$\mathbf{V}_m \oplus \mathbf{W}_m \oplus \mathbf{W}_{m+1} \oplus \ldots \oplus \mathbf{W}_{m+n} = \mathbf{V}_{m+n+1}. \tag{26}$$

Then

$$\begin{aligned} \mathbf{V}_k &= V_k \otimes V_k, \\ \mathbf{W}_k &= (V_k \otimes W_k) \oplus (W_k \otimes V_k) \oplus (W_k \otimes W_k). \end{aligned} \tag{27}$$

Of particular interest is the case $m = 0$ and a subset of functions belonging to the subspaces $\mathbf{V}_k^0 \subset \mathbf{V}_k$ and $\mathbf{W}_k^0 \subset \mathbf{W}_k$, $k \geq 0$, defined as follows:

$$\begin{aligned} \mathbf{V}_{k+1}^0 &= \mathbf{V}_k^0 \oplus \mathbf{W}_k^0, \\ \mathbf{W}_k^0 &= \mathbf{W}_k^h \oplus \mathbf{W}_k^v \oplus \mathbf{W}_k^d, \quad k \geq 0, \end{aligned} \tag{28}$$

where

$$\begin{aligned} \mathbf{V}_k^0 &= \overline{\text{span}\{\phi_{kij}(x,y) = \phi_{ki}(x)\phi_{kj}(y),\ 0 \leq i,j \leq 2^k - 1\}} \\ \mathbf{W}_k^h &= \overline{\text{span}\{\psi_{kij}^h(x,y) = \phi_{ki}(x)\psi_{kj}(y),\ 0 \leq i,j \leq 2^k - 1\}} \\ \mathbf{W}_k^v &= \overline{\text{span}\{\psi_{kij}^v(x,y) = \psi_{ki}(x)\phi_{kj}(y),\ 0 \leq i,j \leq 2^k - 1\}} \\ \mathbf{W}_k^d &= \overline{\text{span}\{\psi_{kij}^d(x,y) = \psi_{ki}(x)\psi_{kj}(y),\ 0 \leq i,j \leq 2^k - 1\}} \end{aligned} \tag{29}$$

The superscripts h, v and d stand for *horizontal*, *vertical* and *diagonal*, respectively [10]. The wavelet expansions will then have the form:

$$f(x,y) = b_{000}\phi_{000}(x,y) + \sum_{k=0}^{\infty} \sum_{i=0}^{2^k-1} \sum_{j=0}^{2^k-1} [a_{kij}^h \psi_{kij}^h(x,y) + a_{kij}^v \psi_{kij}^v(x,y) + a_{kij}^d \psi_{kij}^d(x,y)]. \tag{30}$$

The set of all functions admitting the above wavelet expansions will be denoted as $\mathcal{L}_0^2(\mathbf{R}^2) \subset \mathcal{L}^2(\mathbf{R}^2)$. The space $\mathcal{L}_0^2(\mathbf{R}^2)$ is complete with respect to the usual $\mathcal{L}^2(\mathbf{R}^2)$ metric. The wavelet expansion coefficients may be conveniently arranged in a standard fashion [10, 22]. The arrangement of the first three blocks is shown in Figure 3(a). The blocks $\mathbf{A}_k^h, \mathbf{A}_k^v, \mathbf{A}_k^d$, $k \geq 0$, each contain 2^{2k} coefficients $a_{kij}^h, a_{kij}^v, a_{kij}^d$, respectively. The three collections of blocks

$$\mathbf{A}^h = \bigcup_k^\infty \mathbf{A}_k^h, \quad \mathbf{A}^v = \bigcup_k^\infty \mathbf{A}_k^v, \quad \mathbf{A}^d = \bigcup_k^\infty \mathbf{A}_k^d, \tag{31}$$

comprise the fundamental *horizontal*, *vertical* and *diagonal* quadtrees of the coefficient tree.

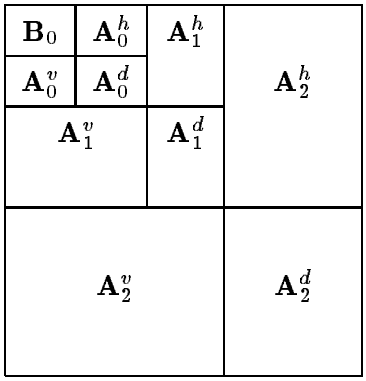

Figure 3(a). Matrix arrangement of two-dimensional wavelet coefficient blocks.

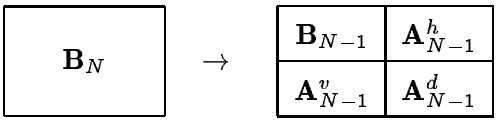

Figure 3(b). Wavelet decomposition algorithm.

Now consider any wavelet coefficient a_{kij}^λ, $\lambda \in \{h, v, d\}$ in this matrix and the unique (infinite) quadtree with this element as its root. We shall denote this (sub)quadtree as A_{kij}^λ. In the Haar case, for a fixed set of indices $\{k, i, j\}$ the three quadtrees A_{kij}^h, A_{kij}^v and A_{kij}^d correspond to the *same spatial portion* of the function or image. This feature was illustrated nicely by Davis [9].

As is well known, the wavelet decomposition algorithm [22, 10] begins with an "image" matrix of coefficients $\mathbf{B}_N$ for some $N > 0$ (e.g. $N = 9$ for a 512×512 pixel array). From $\mathbf{B}_N$ one computes $\mathbf{B}_{N-1}$, $\mathbf{A}_{N-1}^h$, $\mathbf{A}_{N-1}^v$ and $\mathbf{A}_{N-1}^d$. The latter three blocks are stored and $\mathbf{B}_{N-1}$ is then decomposed into $\mathbf{A}_{N-2}^h$, $\mathbf{A}_{N-2}^v$ and $\mathbf{A}_{N-2}^d$. The procedure, depicted schematically in Figure 3(b) above, is continued until one arrives at the single entry blocks $\mathbf{B}_0, \mathbf{A}_0^h, \mathbf{A}_0^v, \mathbf{A}_0^d$. From the matrix in Figure 3(a), $\mathbf{B}_N$ may be reconstructed in reverse fashion. Once a wavelet basis is chosen, these algorithms employ the filters associated with that basis.

Note in closing that the tensorial nature of the basis functions in the $\mathbf{A}_k^\lambda$ leads to the following simple scaling relations:

$$\psi^{\lambda}_{kij}(x,y) = 2^k \psi^{\lambda}_{000}(2^k x - i, 2^k y - j), \qquad \lambda \in \{h, v, d\}. \tag{32}$$

3.2 2D Fractal-Wavelet Transforms

Two-dimensional fractal-wavelet transforms involve mappings of "parent" quadtrees of wavelet expansions to lower "child" quadtrees in the same way as was done for binary trees in the 1D case. For simplicity in presentation and notation, we consider a particular case in which the roots of all parent quadtrees appear in a given block and the roots of all child quadtrees appear in another given block.

Select two integers, the parent and child levels, k_1^* and k_2^*, respectively, with $0 \le k_1^* < k_2^*$. Then for each possible index $0 \le i, j \le 2^{k_2^*} - 1$ define the three sets of affine block transforms:

$$\begin{aligned}
W^h_{ij} &: A^h_{k_1^*, i^h(i,j), j^h(i,j)} \to A^h_{k_2^*, i, j}, \qquad A^h_{k_2^*,i,j} = \alpha^h_{ij} A^h_{k_1^*, i^h(i,j), j^h(i,j)}, \\
W^v_{ij} &: A^v_{k_1^*, i^v(i,j), j^v(i,j)} \to A^v_{k_2^*, i, j}, \qquad A^v_{k_2^*,i,j} = \alpha^v_{ij} A^v_{k_1^*, i^v(i,j), j^v(i,j)}, \\
W^d_{ij} &: A^d_{k_1^*, i^d(i,j), j^d(i,j)} \to A^d_{k_2^*, i, j}, \qquad A^d_{k_2^*,i,j} = \alpha^d_{ij} A^d_{k_1^*, i^d(i,j), j^d(i,j)}.
\end{aligned} \tag{33}$$

These block transforms will comprise a unique IFSW operator M. The use of the indices i^h, j^h, etc. emphasizes that the parent quadtrees corresponding to a given set of child quadtrees $A^h_{k_2^*,i,j}, A^v_{k_2^*,i,j}$ and $A^d_{k_2^*,i,j}$ need *not* be the same. As well, the scaling coefficients $\alpha^h_{ij}, \alpha^v_{ij}$ and α^d_{ij} are *independent*. In the usual fractal-wavelet transforms corresponding to (local) IFSM, e.g. [9],

$$i^h(i,j) = i^v(i,j) = i^d(i,j), \quad j^h(i,j) = j^v(i,j) = j^d(i,j), \quad \text{(common parent blocks)} \tag{34}$$

and

$$\alpha^h_{ij} = \alpha^v_{ij} = \alpha^d_{ij}, \quad \text{(common scaling factors)}. \tag{35}$$

In other words, the h, v and d quadtrees are *not* treated independently.

The "fractal code" associated with an IFSW operator M consists of the following:

1. The parent-child index pair (k_1^*, k_2^*).
2. The wavelet coefficients in blocks $\mathbf{B}_0$ (i.e. b_{000}) and $\mathbf{A}^{\lambda}_k$, $\lambda \in \{h, v, d\}$ for $1 \le k \le k_2^* - 1$. $4^{k_2^*}$ coefficients.
3. The scaling factors α^{λ}_{ij} and parent block indices $(i^{\lambda}(i,j),\ j^{\lambda}(i,j))$ (the i and j indices could, of course, be replaced by a single index) for all elements a^{λ}_{ij} in each of the three blocks $A^{\lambda}_{k_2^*}$. Total number of parameters: (i) $3 \cdot 4^{k_2^*}$ scaling factors, (ii) $2 \cdot 3 \cdot 4^{k_2^*}$ indices.

(At this stage, we are not concerned with questions regarding the practical computer storage of these parameters.)

From the definition of M in Eq. (33), its application to a wavelet coefficient tree leaves the entries in the blocks $\mathbf{B}_0$, $\mathbf{A}^{\lambda}_k$, $\lambda \in \{h, v, d\}$ for $0 \le k \le k_2^* - 1$ unchanged. The first application of M modifies the blocks $\mathbf{A}^{\lambda}_{k_2^*}$. In general, the nth application of M modifies the blocks $\mathbf{A}^{\lambda}_{k_2^*+n-1}$ which then remain unchanged in future iterations (as in the one-dimensional case, cf. Example 1). In practical applications, it suffices to apply the IFSW operator M to the matrix whose entries in blocks $\mathbf{A}^{\lambda}_k$, with $k \ge k_2^*$ are zeroes. Each application of M will produce an additional level of (generally) nonzero blocks, in other words, an additional degree of refinement of the function in terms of its wavelet expansion.

It remains to establish the conditions for contractivity of the IFSW operator M on a suitable complete metric space of wavelet coefficients. Let Q denote the set of all real square-summable quadtrees $\mathbf{c}$, i.e.

$$\mathbf{c} = \{c_{kij} \in \mathbf{R},\ k \geq 0,\ 0 \leq i,j \leq 2^k - 1 \mid \sum_{kij}^{\infty} |c_{kij}|^2 < \infty\} \tag{36}$$

Let d_Q denote the natural l^2 metric on this space, i.e.

$$d_Q(\mathbf{c},\mathbf{d}) = [\sum_{kij}^{\infty}(c_{kij} - d_{kij})^2]^{1/2}, \quad \forall\ \mathbf{c},\mathbf{d} \in Q. \tag{37}$$

Denote the inner product of two quadtrees as follows:

$$\langle \mathbf{c},\mathbf{d}\rangle_Q = \sum_{kij}^{\infty} c_{kij}d_{kij}, \quad \mathbf{c},\mathbf{d} \in Q. \tag{38}$$

We now define a particular subset of Q for which the wavelet blocks $\mathbf{B}_0$ and $\mathbf{A}_k^{\lambda}$ for $\lambda \in \{h,v,d\}, 0 \leq k \leq k_2 - 1$ are fixed. Since the goal will be to approximate functions in $\mathcal{L}_0^2(\mathbf{R}^2)$ via their wavelet expansions, we assume that these fixed blocks correspond to the wavelet coefficients b_{000} and a_{kij}^{λ} of a given function $u \in \mathcal{L}_0^2(\mathbf{R}^2)$. Let $Q(u,k_2^*)$ denote the set of all such quadtrees $\mathbf{c} \in Q$ with blocks in levels $0 \leq k \leq k_2^* - 1$ fixed. Now define the following metric on this space:

$$d_{Q(k_2^*)}(\mathbf{c},\mathbf{d}) = \max_{\lambda,i,j}\ d_Q(C_{k_2^*ij}^{\lambda}, D_{k_2^*ij}^{\lambda}), \quad \mathbf{c},\mathbf{d} \in Q(u,k_2^*), \tag{39}$$

where $C_{k_2^*ij}^{\lambda}$ and $D_{k_2^*ij}^{\lambda}$ denote the (infinite) quadtrees with roots $c_{k_2^*ij}^{\lambda}$ and $d_{k_2^*ij}^{\lambda}$, respectively.

Proposition 1 *The metric space $(Q(u,k_2^*), d_{Q(k_2^*)})$ is complete.*

Proposition 2 *For a given $u \in \mathcal{L}_0^2(\mathbf{R}^2)$ and $k_2^* \geq 1$, the IFSW operator defined in Eq. (33) maps $Q(u,k_2^*)$ into itself. Moreover,*

$$d_{Q(k_2^*)}(M\mathbf{c}, M\mathbf{d}) \leq c_Q\, d_{Q(k_2^*)}(\mathbf{c},\mathbf{d}), \quad c_Q = 2^{k_2^* - k_1^*} \max_{\lambda,i,j} |\alpha_{ij}^{\lambda}|, \tag{40}$$

where $\lambda \in \{h,v,d\}$ and $0 \leq i,j \leq 2^{k_2^*} - 1$.

The following result is a simple consequence of the Banach Contraction Mapping Theorem.

Corollary 1 *If $c_Q < 1$ then there exists a unique $\bar{\mathbf{c}} \in Q(u,k_2^*)$ such that $M\bar{\mathbf{c}} = \bar{\mathbf{c}}$.*

Note how the "spirit of IFS" lives in this transform: The fixed point wavelet tree $\bar{\mathbf{c}}$ is, in effect, a union of scaled copies of its subtrees.

3.3 Simple Examples

The simplest case arises when $(k_1^*, k_2^*) = (0,1)$. Schematically we have the block transformation

$$M : \begin{array}{|c|c|}\hline B_{000} & A^h_{000} \\ \hline A^v_{000} & A^d_{000} \\ \hline \end{array} \rightarrow \begin{array}{|c|c|c|c|}\hline b_{000} & a^h_{000} & \alpha^h_{00}A^h_{000} & \alpha^h_{01}A^h_{000} \\ \hline a^v_{000} & a^d_{000} & \alpha^h_{10}A^h_{000} & \alpha^h_{11}A^h_{000} \\ \hline \alpha^v_{00}A^v_{000} & \alpha^v_{01}A^v_{000} & \alpha^d_{00}A^d_{000} & \alpha^d_{01}A^d_{000} \\ \hline \alpha^v_{10}A^v_{000} & \alpha^v_{11}A^v_{000} & \alpha^d_{10}A^d_{000} & \alpha^d_{11}A^d_{000} \\ \hline \end{array} . \tag{41}$$

The condition $|\alpha^\lambda_{ij}| < 1/2$ guarantees the contractivity of M. The fixed point of this operator will have the entry B_{000} as well as the component quadtrees $\bar{A}^\lambda_{000}$, $\lambda \in \{h,v,d\}$. It will represent the wavelet expansion of the function $\bar{u}$ where

$$\bar{u} = \bar{u}_0 + \bar{v}, \quad \bar{u}_0 = b_{000}\phi_{000}, \tag{42}$$

$$\bar{v} = \bar{v}^h + \bar{v}^v + \bar{v}^d, \tag{43}$$

$$\bar{v}^\lambda = \sum_{i,j=0}^{1} \bar{v}^\lambda_{ij}, \quad \lambda \in \{h,v,d\}. \tag{44}$$

Each component $\bar{v}^\lambda$ satisfies the relations

$$\bar{v}^\lambda(x,y) = \theta^\lambda(x,y) + \sum_{i,j=0}^{1} 2\alpha^\lambda_{ij}\bar{v}^\lambda(w^{-1}_{ij}(x,y)) \tag{45}$$

where $\theta^\lambda(x,y) = a^\lambda_{000}\psi^\lambda_{000}$ and

$$w_{ij}(x,y) = \left(\frac{x}{2} + \frac{i}{2}, \frac{y}{2} + \frac{j}{2}\right), \quad 0 \le i,j \le 1. \tag{46}$$

The three equations in (45) comprise a recurrent IFSM with condensation functions. Note that there is no mixing between the orthogonal h, v and d subspaces. (One could consider generalizations of the IFSW in (33) which would permit such mixing.)

Case 1: In the special case that $\alpha^\lambda_{ij} = \alpha_{ij}$, $\lambda \in \{h,v,d\}$, then the three equations in (45) can be added together to give

$$\bar{v}(x,y) = \theta(x,y) + \sum_{i,j=0}^{1} 2\alpha_{ij}\bar{v}(w^{-1}_{ij}(x,y)), \tag{47}$$

corresponding to an IFSM with condensation function $\theta = \theta^h + \theta^v + \theta^d$.

In the Haar wavelet case, the above equation could be rewritten as a simple four-map IFSM with affine grey-level maps (i.e. without a condensation function):

$$\bar{v}(x,y) = \sum_{i,j=0}^{1} [2\alpha_{ij}\bar{v}(w^{-1}_{ij}(x,y)) + \beta_{ij}]. \tag{48}$$

Here, the support of the fixed point function $\bar{u}$ is $[0,1]^2$. This demonstrates the connection between the usual IFSM and fractal-wavelet transforms in the Haar basis.

Case 2: Now consider the more general case in which the α_{ij}^{λ} are not necessarily equal for each i, j pair. As in the first case, add the three equations in (45) and write the result as

$$\bar{v}(x,y) = \theta(x,y) + 2\sum_{i,j=0}^{1}[\alpha_{ij}\bar{v}(w_{ij}^{-1}(x,y)) + \delta_{ij}\bar{v}^h(w_{ij}^{-1}(x,y)) + \gamma_{ij}\bar{v}^v(w_{ij}^{-1}(x,y))], \qquad (49)$$

where

$$\alpha_{ij} = \alpha_{ij}^d, \quad \delta_{ij} = \alpha_{ij}^h - \alpha_{ij}^d, \quad \gamma_{ij} = \alpha_{ij}^v - \alpha_{ij}^d. \qquad (50)$$

This may be considered as a perturbation of the recurrent IFSM with condensation function in Eq. (47). It is convenient to consider the "offdiagonal" components $\bar{v}^h$ and $\bar{v}^v$ as perturbations since they produce horizontal and vertical gradations in the shading, as we show in the examples below.

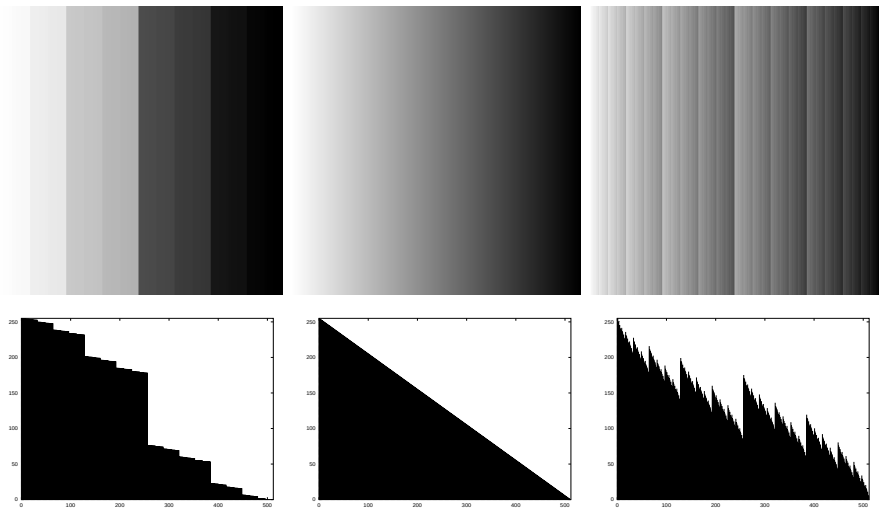

Figure 4. Attractor functions for IFSW of Eq. (41) with $\alpha_{ij}^h = \alpha_{ij}^d = 0$, $a_{000}^h = a_{000}^d = 0$ and $a_{000}^v = 1$ in the Haar wavelet basis: (a) $\alpha_{ij}^v = 0.15$, (b) $\alpha_{ij}^v = 0.25$, (c) $\alpha_{ij}^v = 0.35$. Beneath each attractor is plotted a sample cross section of the function values.

Even in the simple case $(k_1^*, k_2^*) = (0,1)$, the number of "degrees of freedom" in the transformations in Eq. (41) is large. It is instructive to examine the simple cases in which only one of the three principal quadtrees, h, v or d, is nonzero. In this way, we obtain an idea of how these fundamental components operate. As well, we may examine the role of the wavelet basis used. In the following examples, the range of values assumed by the attractor function was scaled to the interval $[0, 255]$ and plotted as a 512×512 pixel image with 256 shades (8 bits/pixel) of grey. Figures 4(a)-(c) show plots of attractors for which $c_{000}^h = c_{000}^d = 0$, $c_{000}^v = 1$, the h and d scaling factors are zero and $\alpha_{ij}^v = 0.15, 0.25$ and 0.35, respectively. In all three cases, the attractor shows a gradation of shading in the horizontal direction. Below each of the three attractors is shown a cross-sectional plot of their pixel values. The horizontal gradation is due to the behaviour of the "root wavelet" $\psi_{000}^v(x,y) = \psi(x)\phi(y)$ whose qualitative property is shown in Figure 5(b). The degree of shading is dependent upon the scaling factors. The cross-sectional plots are attractor functions of appropriate one-dimensional IFSM/IFSW in the Haar basis (cf. Figure 1(a)).

Identical vertical gradations of the image are produced when the v and d scaling factors are set to zero and the α_{ij}^h factors are allowed to assume the above values. The resulting

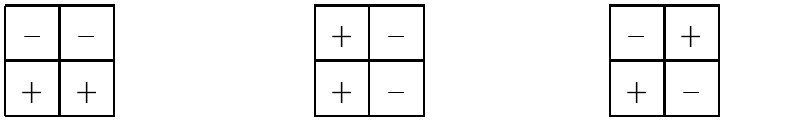

(a) $\psi^h = \phi(x)\psi(y)$ (b) $\psi^v = \psi(x)\phi(y)$ (c) $\psi^d = \psi(x)\psi(y)$

Figure 5. Qualitative properties of the principal Haar wavelet basis functions.

images are simply rotations of Figures 4(a)-(c) by $\pi/2$. This is expected from the qualitative behaviour of the wavelet $\psi^h_{000}(x,y) = \phi(x)\psi(y)$ shown in Figure 5(a).

The horizontal and vertical gradations observed above are quite similar to the "ramping" that is produced by the multiplication of grey-level values by an x or y coordinate in the place-dependent IFSM or Bath Fractal Transform - see Appendix A.

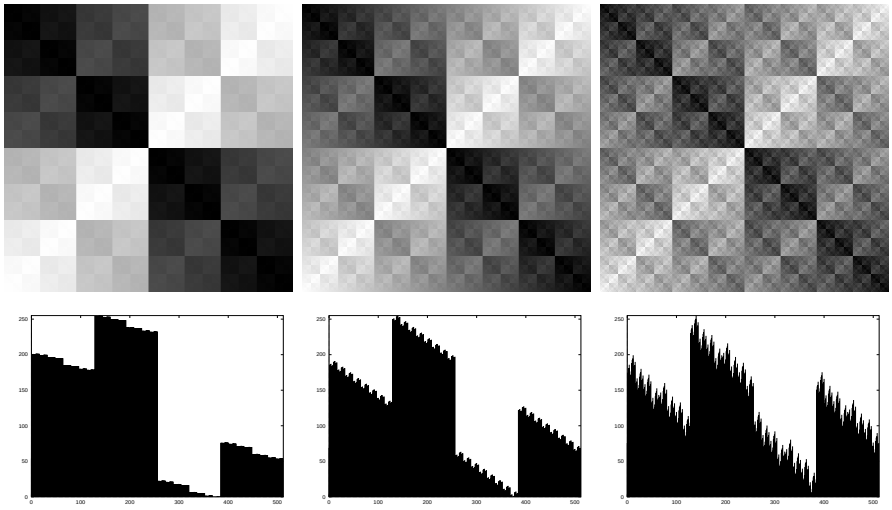

Figure 6. Attractor functions for IFSW of Eq. (41) with $\alpha^h_{ij} = \alpha^v_{ij} = 0$, $a^h_{000} = a^v_{000} = 0$ and $a^d_{000} = 1$ in the Haar wavelet basis: (a) $\alpha^d_{ij} = 0.15$, (b) $\alpha^d_{ij} = 0.25$, (c) $\alpha^d_{ij} = 0.35$. Beneath each attractor is plotted a sample cross section of the function values.

A quite different pattern is produced when the v and h components are set to zero and only the d components are operating. Figures 6(a)-(c) show the attractor functions for the cases $\alpha^d_{ij} = 0.15, 0.25$ and 0.35, respectively. Figures 7(a)-(c) show the attractor functions which correspond to the parameter values in Figures 4(a)-(c) in the Coifman-6 wavelet basis.

4 Fractal-Wavelet Transforms and the Inverse Problem

Fractal-based approximation methods are based on the following strategy. Let (Y, d_Y) denote a complete metric space whose elements represent the "images" we wish to approximate. (For example, Y could be composed of sets, measures, functions or distributions.) Also let $Con(Y)$ denote the set of contraction mappings on Y, that is,

$$Con(Y) = \{f : Y \to Y \quad | \quad d_Y(f(y_1), f(y_2)) \leq c_f d_Y(y_1, y_2), \\ \forall y_1, y_2 \in Y \quad \text{for some} \quad c_f \in [0,1)\}. \tag{51}$$

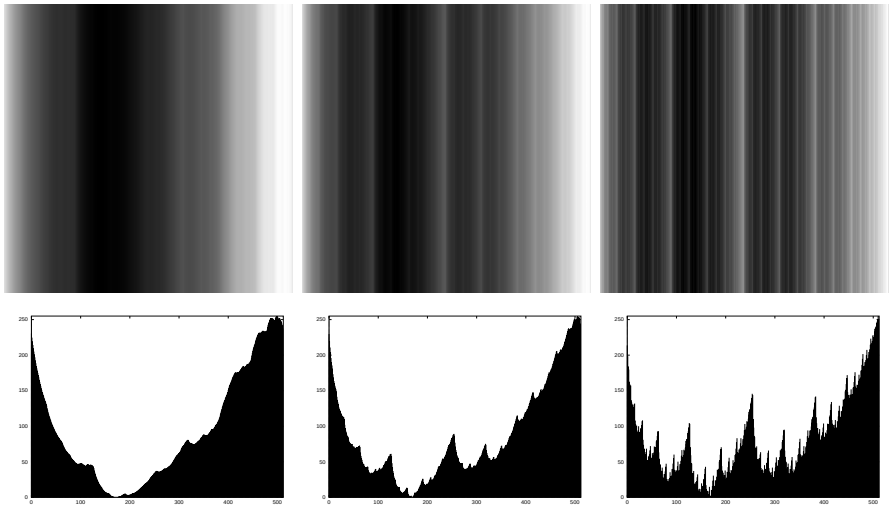

Figure 7. Attractor functions for IFSW of Eq. (41) with $\alpha^h_{ij} = \alpha^d_{ij} = 0$, $a^h_{000} = a^d_{000} = 0$ and $a^v_{000} = 1$ in the periodized Coifman-6 (6 tap) wavelet basis: (a) $\alpha^v_{ij} = 0.15$, (b) $\alpha^v_{ij} = 0.25$, (c) $\alpha^v_{ij} = 0.35$. Beneath each attractor is plotted a sample cross section of the function values. These plots should be compared with their Haar wavelet counterparts in Figure 4.

Now suppose that $y \in Y$ is a "target" image. Given an acceptable error $\epsilon > 0$ one seeks to find (if possible!) a contraction map $f_\epsilon \in Con(Y)$ whose fixed point $\bar{y}_\epsilon$ approximates y with ϵ, i.e. $d_Y(\bar{y}_\epsilon, y) < \epsilon$.

In fractal image compression, it is the contraction mapping f_ϵ that is stored in the computer. Reconstruction of the approximation $\bar{y}_\epsilon$ to y is achieved by the iteration sequence $y_{n+1} = f_\epsilon y_n$. Banach's Contraction Mapping Theorem guarantees that $d_y(y_n, \bar{y}_\epsilon) \to 0$ as $n \to \infty$ for any $y_0 \in Y$. (For example, let y_0 be a blank or black screen, i.e. $y_0 = 0$.)

Most fractal-based methods of approximation are based on the "Collage Theorem" [1], a simple corollary of Banach's Theorem:

Theorem 1 *Let (Y, d_Y) be a complete metric space. For any $y \in Y$ and $f \in Con(Y)$,*

$$d_Y(y, \bar{y}) \leq \frac{1}{1 - c_f} d_Y(f(y), y) \tag{52}$$

where $\bar{y} = f(\bar{y})$ is the unique fixed point of f and c_f is its contraction factor.

If y is the target image, then making the *collage distance* $d_Y(f(y), y)$ small (by looking for "good" f's) forces $d_Y(y, \bar{y})$ to be small (to within a multiplicative factor). The inverse problem for fractal approximation may then be rephrased as follows:

> Given a $y \in Y$ and a $\delta > 0$, find a contraction mapping $f \in Con(Y)$ such that $d_Y(f(y), y) < \delta$.

This study is concerned with an *indirect* inverse problem [15, 36]: Instead of directly constructing approximations to an image function, we construct approximations to a faithful representation of the function, namely its wavelet expansion. (Inverse problems employing Fourier transforms of functions or moments of probability measures may also be formulated [15, 36].) Here, the space (Y, d_Y) will be a suitable subset of Q the set of all square-summable 2D wavelet coefficients. The relevant contraction maps in $Con(Y)$ will be the

IFSW operators defined in Eq. (33). In what follows we let $v \in \mathcal{L}_0^2(\mathbf{R}^2)$ denote the target image function and $\mathbf{a} \in \mathbf{Q}$ its wavelet expansion (cf. Eq. (36)). We seek to approximate $\mathbf{a}$ by the fixed point $\bar{\mathbf{a}}$ of a contractive IFSW operator. It remains to specify the parent and child indices k_1^* and k_2^*, respectively. Then $(Y, d_Y) = (Q(v, k_2^*), d_{Q(k_2^*)})$. Note that $\mathbf{a} \in Q(v, k_2^*)$.

From the Collage Theorem, the approximation problem involves the minimization of the following collage distances between subtrees:

$$\begin{aligned} \Delta &= d_{Q(k_2^*)}(\mathbf{a}, M\mathbf{a}) \\ &= \max_{\lambda,i,j} \Delta_{ij}^{\lambda}, \end{aligned} \tag{53}$$

where

$$\Delta_{ij}^{\lambda} = d_{Q(k_2^*)}(A_{k_2^* ij}^{\lambda}, \alpha_{ij}^{\lambda} A_{k_1^* i^{\lambda}(i,j) j^{\lambda}(i,j)}^{\lambda}), \quad \lambda \in \{h, v, d\}, \quad 0 \le i, j \le 2^{k_2^*} - 1, \tag{54}$$

In order for M to be contractive, the scaling parameters must satisfy the constraint $|\alpha_{ij}^{\lambda}| < \alpha_{\max} = 2^{k_1^* - k_2^*}$. In Eqs. (53) and (54), the minimization of the collage distance has been performed with respect to a fixed set of parent indices $(i^{\lambda}(i,j), j^{\lambda}(i,j))$. Clearly, the optimal result is achieved when the minimization is done with respect to all possible parent indices $0 \le i^{\lambda}(i,j), j^{\lambda}(i,j) \le 2^{k_2^*} - 1$, referred to as a *full search* of parent blocks.

In practical computations, e.g. images, one necessarily works with truncated wavelet trees, typically the matrix $\mathbf{B}_9$ for a 512×512 pixel image. As in the case of normal fractal-based compression methods, a variety of strategies for parent block searching may be employed, including:

1. full searching of all possible parent blocks,
2. restricted searching, either in a specified neighbourhood of the child block or among a subset of parent blocks belonging to a prescribed class,
3. no searching - usually the block containing the child block is chosen as the parent.

Clearly, travelling down this list represents a decrease in computational (and coding) cost but at the expense of decreased accuracy.

The minimization of the squared collage distances $(\Delta_{ij}^{\lambda})^2$ in Eq. (53) is a quadratic programming problem with constraints. There is no guarantee that an optimal scaling factor α_{ij}^{λ} exists in the interval $(-\alpha_{\max}, \alpha_{\max})$. As such, an upper "cutoff" $0 < \alpha_c < \alpha_{\max}$ must be introduced in practice so that the feasible set of scaling parameters is the closed interval $[-\alpha_c, \alpha_c]$. Most, if not all, practical applications avoid such a computationally expensive procedure and settle for a minimization of the squared collage distance (omitting the λ index)

$$\Delta_{ij}^2 = \langle A_{k_2^* ij} - \alpha_{ij} A_{k_1^* i' j'}, A_{k_2^* ij} - \alpha_{ij} A_{k_1^* i' j'} \rangle_Q \tag{55}$$

by "least-squares". The optimal scaling factor is

$$\bar{\alpha}_{ij} = \frac{\langle A_{k_2^* ij}, A_{k_1^* i' j'} \rangle_Q}{\langle A_{k_1^* i' j'}, A_{k_1^* i' j'} \rangle_Q} \tag{56}$$

and the minimum squared collage distance is

$$\Delta_{ij}^2 = \langle A_{k_2^* ij}, A_{k_2^* ij} \rangle_Q - \bar{\alpha}_{ij} \langle A_{k_2^* ij}, A_{k_1^* i' j'} \rangle_Q. \tag{57}$$

In this case, it is *not* guaranteed that $|\bar{\alpha}_{ij}| < \alpha_{\max}$. This fact is usually overlooked in practical applications where computations are performed only to a finite resolution, e.g. to $\mathbf{B}_9$. (In fact, as will be shown below, irregular regions of an image, e.g. edges, will almost surely imply the existence of scaling factors with large magnitudes. This is a complicated issue involving the approximation of images and edges at finite resolution and will be dealt with only partially here.)

We conclude this section with an important property that provides the basis of fractal-based approximation methods, namely, the continuity of fixed points with respect to contraction maps [5]. Given a compact metric space (Y, d_Y), define the following metric on the space $Con(Y)$:

$$d_{Con(Y)}(f,g) = \sup_{y \in Y} d(f(y), g(y)), \quad f, g \in Con(Y). \tag{58}$$

(Note that the metric space $(Con(Y), d_{Con(Y)})$ is not necessarily complete.)

Theorem 2 *Let (Y, d_Y) be a compact metric space and $f, g \in Con(Y)$ with fixed points $\overline{y}_f$ and $\overline{y}_g$, respectively. Then*

$$d_Y(\overline{y}_f, \overline{y}_g) < \frac{1}{1 - \min(c_f, c_g)} d_{Con(Y)}(f,g), \tag{59}$$

where c_f, c_g denote the contractivity factors of f and g, respectively.

In other words, the "closer" f and g are to each other, the closer are their respective fixed points $\overline{y}_f$ and $\overline{y}_g$. This result, the proof of which involves a simple application of the triangle inequality, is a generalization of Barnsley's "continuity with respect to a parameter" [1]. It was used to derive continuity properties of IFS attractors and IFSP invariant measures [5]. *Although never stated explicitly, fractal compression algorithms depend on this property. Minimization of the collage distance involves a variation of fractal transform parameters.*

Following Proposition 2 of Section 3.2, consider the subset of IFSW operators which share a fixed set of indices $i^\lambda(i,j), j^\lambda(i,j)$, $\lambda \in \{h, v, d\}$. In other words, only the scaling coefficients α_{ij}^λ are allowed to vary. Let M_1 and M_2 be two IFSW operators from this set with scaling factors $\alpha_{ij}^\lambda(1)$ and $\alpha_{ij}^\lambda(2)$, respectively. From [5], a natural distance between these operators is given by

$$d_{Con(Q(k_2^*))} = \max_{\lambda,i,j} |\alpha_{ij}^\lambda(2) - \alpha_{ij}^\lambda(1)|. \tag{60}$$

In addition to establishing the continuity of fixed points of such operators with respect to the scaling parameters, this metric could be considered to obtain estimates of quantization errors.

5 Some Applications to Images

Some results of fractal-wavelet approximation and compression will now be presented. We emphasize that the primary purpose of this preliminary study is to show the relative accuracy of the various approximations. The actual exercises employed for *image compression* in this study are quite rudimentary. For example, no special effort has been taken to ensure optimal allocation of bits of storage. As well, we restrict our attention to a fixed parent/child block structure, i.e. no *adaptive* partitioning has been employed.

Figure 8. "Standard" fractal-wavelet approximations to the 512×512 pixel Lena image with $(k_1^*, k_2^*) = (5, 6)$, in which $\alpha_{ij}^h = \alpha_{ij}^v = \alpha_{ij}^d$, same parents. Left: Haar basis (corresponds to usual IFSM with 16×16 parent blocks $\rightarrow 8 \times 8$ child blocks); $d_2 = 8.2$, PSNR= 29.8. Right: (periodized) Coifman-6 basis; $d_2 = 7.9$, PSNR= 30.2.

Obviously, compression and accuracy are competing features. Fractal-wavelet approximations to arbitary accuracy may be obtained by letting the parent block index k_1^* become arbitrarily large. However, this is suicidal from the viewpoint of compression. One may try to achieve the maximum compression for a given allowable accuracy or *vice versa*. In this study, we examine the interplay of compression and accuracy for various forms of generalized 2D IFSW operators.

The computations reported here involve the approxmation of the standard "Lena" image, 512×512 pixels, 8 bits per pixel. Two measures of the accuracy of approximation will be used: (a) an $\mathcal{L}^2$ distance between images and (b) the "peak signal-to-noise ratio" (PSNR) in decibel (dB) units, a standard measure in image compression. For two image functions u, v with pixel values $0 \leq u_{ij}, v_{ij} \leq 255$, $1 \leq i, j \leq 512$, the $\mathcal{L}^2$ distance will be defined as follows:

$$d_2(u, v) = \frac{1}{512} \left[\sum_{i,j} [u_{ij} - v_{ij}]^2 \right]^{1/2} . \tag{61}$$

If we consider u to be an approximation to the target image v then the PSNR is given by

$$\text{PSNR (dB)} = 20 \log_{10} \left[\frac{255}{d_2(u, v)} \right] . \tag{62}$$

In order to facilitate a translation between the two measures, a small table of values is given below.

d_2	6.0	7.0	8.0	9.0	10.0	12.0	14.0
PSNR	32.57	31.23	30.10	29.05	28.13	26.55	25.21

Simple Fractal-Wavelet Calculations. We begin with a look at "standard" IFSW approximations to the Lena image used in the literature to date, in which the h, v and d quadtrees share the same scaling factor α_{ij} and parent block indices. (This is achieved by "collaging" the three blocks simultaneously with respect to the same parent index.) The

approximations in Figure 8 correspond to the parent-child root blocks $(k_1^*, k_2^*) = (5, 6)$. Figure 8(a) corresponds to the nonoverlapping Haar case, which is identical to the usual "local" IFSM or Jacquin block encoding scheme where 16×16 pixel parent blocks are mapped onto 8×8 pixel child blocks. (Recall that a partitioning into 8×8 pixel blocks is the JPEG-DCT standard.) Figure 8(b) is the result achieved in the Coifman-6 basis. It provides a better approximation with less blockiness, one of the original motivations for the use of the IFSW with generalized wavelet bases. In both cases, a full search of all possible parent quadtrees was made.

The approximation yielded by the standard fractal block encoding scheme in Figure 8(a) at the $(5, 6)$ parent-child block level may seem acceptable, and Figure 8(b) even more so, but the compression ratios are rather moderate. Roughly, a child block requiring 64 pixels $\times 8$ bits/pixel is replaced by a parent index pair ($5 + 5 = 10$ bits at most) and the scaling coefficient α (possibly 4 bits). This, along with the storage of the parent wavelet coefficients, implies a compression ratio of about $25 : 1$. Some improvement in quantization as well as more effective coding techniques (e.g Huffman, arithmetic) may be able to push this ratio to 30 or 40:1. (The Bath Fractal Transform employs three scaling parameters in each grey-level map with apparently no loss in compression. Some of the storage originally allocated for parent indices may be sacrificed for the extra scaling parameters since a lesser search of parent blocks is required for comparable accuracy.)

Calculations at lesser refinement. In an attempt to (1) increase the compression ratio and (2) examine the relative effectiveness of various fractal-wavelet schemes, we now examine the approximation of Lena at a less refined parent-child block pairing, namely, $(k_1^*, k_2^*) = (4, 5)$. (For the usual nonoverlapping Haar-based IFSM, this would correspond to 32×32 pixel blocks being mapped to 16×16 blocks.) Some results are shown in Figure 9. Figures 9(a) and 9(b) (top) are the less-refined counterparts of Figures 8(a) and 8(b), respectively, i.e. same scaling factors and parent blocks for h, v and d quadtrees, Haar and Coifman-6 basis. Figures 9(c) and 9(d) (bottom) are generalized IFSW approximations in which the h, v and d quadtrees have independent scaling factors and parents. The improvement in the approximations is quite obvious, but at the expense of more fractal code parameters.

The storage requirements for independent scaling factors and parent indices in the generalized IFSW method greatly diminish the compression ratio. A suitable compromise that increases the compression at some expense of accuracy is achieved if we employ the same parent block but three independent scaling factors. Figures 10(a), 10(b) (top entries) and 10(c) (bottom left) show the results of this approach using the Haar, Coifman-6, and Daubechies-10 wavelet bases. Note the steady improvement in the approximation. Also shown for comparision is an approximation yielded by the place-dependent IFSM or "Bath Fractal Transform". As with the IFSW transform, the BFT employs three scaling parameters for each child cell - see Eq. (78) in Appendix A. Blockiness is also reduced by the BFT in a rather satisfactory manner. It is interesting to note that the BFT and Haar IFSW transforms yield results with roughly the same error. There is, however, a greater flexibility with the IFSW transform since a variety of wavelet basis sets may be employed.

Simple attempts at compression. The results in Figure 10 demonstrate a moderate image compression since both the parent wavelet coefficients and scaling coefficients were computed as single precision real numbers. We now present the results of some rather elementary compression techniques which have employed very simple quantization of the fractal code parameters. The stored wavelet coefficients in blocks $\mathbf{A}_k^\lambda$, $1 \le k \le k_2^* - 1$ were uniformly quantized (midriser) between their maximum and minimum values. The b_{000}

Figure 9. IFSW approximations with $(k_1^*, k_2^*) = (4, 5)$. **Top:** "Standard" fractal-wavelet in which $\alpha_{ij}^h = \alpha_{ij}^v = \alpha_{ij}^d$, same parents. Left: Haar basis (usual IFSM), $d_2 = 13.5$, PSNR= 25.6. Right: Coifman-6 basis, $d_2 = 13.0$, PSNR= 25.8. **Bottom:** Three child blocks $A_{k_2^* ij}^{\lambda}$ have independent scaling factors α_{ij}^{λ} and parents. Left: Haar basis, $d_2 = 11.4$, PSNR= 27.0. Right: Coifman-6 basis, $d_2 = 10.7$, PSNR= 27.6.

Figure 10. Top: Generalized IFSW approximations with $(k_1^*, k_2^*) = (4, 5)$. The three child blocks $A^{\lambda}_{k_2^* ij}$ have independent scaling factors α^{λ}_{ij} but a common parent block. Left: Haar basis, $d_2 = 12.5$, PSNR= 26.2. Right: Coifman-6 basis, $d_2 = 11.8$, PSNR= 26.7. **Bottom:** Left: $(4, 5)$ IFSW approximation as above but with Daubechies-10 basis, $d_2 = 11.4$, PSNR= 27.0. Right: Place-dependent IFSM (Bath Fractal Transform). 32×32 pixel parent cells mapped to 16×16 pixel child cells. Each child cell has three scaling factors. $d_2 = 12.5$, PSNR= 26.2. The compression ratios (unoptimized) are roughly 45:1.

		n_1				
		16	10	8	6	4
	8	26.67	26.66	26.64	26.33	22.59
	6	26.60	26.59	26.56	26.24	22.57
n_2	4	26.07	26.07	26.05	25.82	22.31
	3	25.00	25.01	24.97	24.71	21.53
	2	19.59	19.60	19.56	19.36	17.41

PSNR (dB)

		n_1				
		16	10	8	6	4
	8	42.7	48.8	51.2	53.9	56.9
	6	48.8	56.9	60.2	64.0	68.3
n_2	4	56.9	68.3	73.1	78.8	85.3
	3	62.1	75.9	81.9	89.1	97.5
	2	68.3	85.3	93.1	102.4	113.8

Compression Ratio R

Table 1. Results of IFSW approximation of "Lena" where $(k_1^*, k_2^*) = (4, 5)$ for various quantizations of stored wavelet coefficients and scaling parameters. For a fixed index (i, j), the three child quadtree blocks A_{ij}^{λ}, $\lambda \in \{h, v, d\}$ are scaled independently but share a common parent block. Full search of parent blocks. Periodized Coifman-6 basis. The maximum PSNR value (no quantization error) is 26.7: Figure 10, top right.

wavelet coefficient, which stands out at a rather large magnitude, was stored separately. The scaling factors α_{ij}^{λ} were quantized uniformly (midriser) with truncation. In low-bit cases where $n_1, n_2 \leq 4$, a truncation value of 1.25 was used. This value was found experimentally to yield the best approximations. It is naturally related to the variance of the α_{ij}^{λ} scaling coefficients, found to be roughly 0.96. For higher bit allocations larger truncation values up to 2.5 were used. (Note that no results using entropic coding of the fractal code parameters or sophisticated "bit allocation" are reported here. Some preliminary calculations have shown that a simple Huffman coding of the parameters can increase the compression ratios by a factor of more than 1.5.)

We simply assume that n_1 bits of storage are used for each parent wavelet coefficient and n_2 bits for each scaling coefficient α_{ij}^{λ}. As before, we assume that corresponding child blocks in the h, v and d quadtrees *share the same parent block*. Unless otherwise indicated, a full search of parent blocks is made so that each $(i^{\lambda}, j^{\lambda})$ parent index pair requires $2k_1^*$ bits. Then a "raw" or unoptimized compression ratio R will be defined as the ratio of bits required to store "Lena" , i.e. $512^2 \times 8 = 2^{21}$, to the number of bits required to store the fractal code:

$$R = \frac{2^{21}}{4^{k_2^*}(n_1 + 3n_2 + 2k_1^*)}. \tag{63}$$

This value is also applicable to the Bath Fractal Transform of Figure 10.

Table 1 summarizes PSNR values as well as compression ratios for a number of (n_1, n_2) cases where $(k_1^*, k_2^*) = (4, 5)$ in the periodized Coifman-6 basis. For each child block, a full search of parent blocks was performed.

These tables reveal that there is virtually no reduction in accuracy as the number of bits n_1 allocated for the stored parent wavelet coefficients is reduced from 16 to 8. A marked reduction is observed, however, as n_1 decreases from 5 to 4. As expected, there is a reduction in accuracy as the the number of bits n_2 allocated for the α_{ij} scaling parameters decreases. A significant reduction is observed as as n_2 decreases from 3 to 2. Clearly, there exist minimal bit-rates for these two sets of fractal code parameters. Figure 11 shows the attractors for (a) $(n_1, n_2) = (10, 6)$ and (b) $(n_1, n_2) = (6, 4)$.

For purposes of comparison, Table 2 presents PSNR values obtained for a range of compression ratios using the "Set Partitioning in Hierarchical Trees" (SPIHT) algorithm

Figure 11. Generalized IFSW approximations with $(k_1^*, k_2^*) = (4, 5)$ with quantization. The three child blocks $A^{\lambda}_{k_2^* ij}$ have independent scaling factors α^{λ}_{ij} but a common parent block. Left: $(n_1, n_2) = (10, 6)$, PSNR= 26.59, $R = 56.9$. Right: $(n_1, n_2) = (6, 4)$, PSNR= 25.82, $R = 78.8$.

[31]. This wavelet compression method is probably one of the most powerful to date. With some additional optimization of the storage (e.g. Huffman coding), and adaptive partitioning, the unoptimized results of this study could be improved to compare favorably with the results of Table 2.

C.R.	30:1	35.0	40:1	45:1	50:1	55.1	60:1	70:1
PSNR	34.32	33.63	33.10	32.61	32.13	31.72	31.36	30.70

Table 2. PSNR vs. compression ratio for the "Lena" image using the SPIHT method.

More than one parent per child. Finally, in the spirit of developing other "collaging strategies" with these fractal-wavelet transforms, one may consider the mapping of more than one parent quadtree onto a child quadtree. In the simplest case of two parents, the minimization of the square of the collage distance (omitting the λ index),

$$\Delta_{ij} = d_{Q(k_2^*)}(A_{k_2^* ij}, \alpha_{ij,1} A_{k_1^* i_1(i,j) j_1(i,j)} + \alpha_{ij,2} A_{k_2^* i_2(i,j) j_2(i,j)}), \tag{64}$$

by least-squares leads to a set of linear equations in the two unknown scaling factors $\alpha_{ij,1}$ and $\alpha_{ij,2}$. The computational time required for two simultaneous full searches becomes quite large: For the case $(k_1^*, k_2) = (4, 5)$, a full search for both parents (omitting, of course, repetitions) requires over 20 minutes of CPU time in total, as opposed to typically 40-50 seconds for the full searching of one parent. One possible simplification is as follows: given a child quadtree, perform (a) a full search for one parent along with (b) a restricted search for the other parent, limited to quadtrees which lie within a prescribed neighbourhood $n_p \geq 0$ of the quadtree containing the child quadtree. Clearly, if $n_p = 0$, then the second parent is restricted to be the quadtree containing the child. Better approximations are expected as n_p increases.

For the case $(k_1^*, k_2^*) = (4, 5)$ *with no quantization*, the maximum PSNR values obtained for the first four cases are given below, along with CPU times (unoptimized FORTRAN code):

Figure 12. Generalized IFSW approximations with $(k_1^*, k_2^*) = (4, 5)$: Two parents mapped onto a single child block. Full search for one parent. Search for other parent restricted to quadtrees which lie within a neighbourhood of two quadtrees from the parent block containing the child. (a) No quantization, PSNR = 27.99. (b) $(n_1, n_2) = (10, 4)$ quantization, PSNR = 26.87, $R = 45.1$.

n_p	0	1	2	3
PSNR	27.25	27.74	27.99	28.17
CPU sec.	53	201	492	933

As expected, the introduction of a second parent yields approximations of higher accuracy than the maximum PSNR value of 26.7 obtained with a (4,5) single-parent fractal-wavelet transform of Lena. The accuracy of the approximations increases with the size n_p of the neighbourhood searched but at a rapidly growing computational expense. As well, the improvements in accuracy for $n_p > 3$ are small and diminish rapidly. The PSNR accuracy corresponding to a full search, $n_p = 15$, is 28.91. These fractal-wavelet transforms with two parents are also sensitive to the quantization, especially the truncation value. Two approximations obtained for the $n_p = 2$ case are shown in Figure 12: (a) unquantized, (b) $(n_1, n_2) = (10, 4)$ quantization, with PSNR = 26.87. The compression ratio of 45.1 is slightly less than that for a (10,8) quantization for a single parent (48.8 in Table 1), since 4 bits are needed to code the location of the second parent.

6 IFSW and Extrapolation of Wavelet Coefficients

The fractal-wavelet transforms discussed in this paper perform an IFS-type operation of scaling and copying of wavelet coefficient subtrees onto lower subtrees in a parallel manner. The net result of the IFSW operation is an extrapolation of wavelet coefficients which is produced by the iteration of the fractal transform operator. We start with the the stored wavelet coefficient blocks $\mathbf{A}_k^\lambda$, $1 \le k \le k_2^* - 1$. This truncated wavelet expansion is the "zeroth-order" approximation to the image. The ith application of the fractal-transform operator produces the set of higher resolution blocks $\mathbf{A}_{k_2^*+i}^\lambda$, $i = 1, 2, \ldots$. As shown below, the asymptotic geometric decay/growth of the extrapolated wavelet coefficients is characterized by the scaling coefficients α_{ij}^λ. Recall that these coefficients are determined by the least-squares "collaging" of high-frequency wavelet coefficients by their low-frequency counterparts. We now outline two particular applications of this extrapolation process.

6.1 Regularity/Irregularity Properties

There is a natural connection between the affine of the fractal-wavelet transform and the scaling relationships for wavelet transforms in regions of regularity and irregularity. In the case of image functions, irregularities are typically manifested as edges; regular regions are areas of smoothness. An image is fundamentally characterized by its edges which typically define boundaries of objects in it. Moreover, such sets of irregularity usually comprise a rather small fraction of the total area of the image. As such, there has been much work on the reconstruction of images from the large information contained in edge regions. Recently, Mallat and coworkers have used scaling relationships of wavelet transforms to reconstruct images with claims of high data compression [24, 25, 16].

We now show roughly how the scaling coefficients α_{ij} of the fractal-wavelet transform can be related to regularity/irregularity features of the image being represented. This discussion will be kept as brief and simple as possible and, for simplicity, will be restricted to the one-dimensional case. First, consider an "image function" $f(x)$ on $\mathbf{R}$. Let n be a nonnegative integer and $n \leq \beta \leq n+1$. Suppose that for a point $x_0 \in \mathbf{R}$, there exist a constant $K > 0$ and an nth degree polynomial $P_{n,x_0}(x) = \sum_{k=0}^{n} a_k(x_0)(x - x_0)^k$ (the a_k depend on the x_0 as they do for Taylor polynomials) such that

$$|f(x) - P_{n,x_0}(x)| \leq K|x - x_0|^\beta \tag{65}$$

for all x in a neighbourhood N of x_0. Then f is said to be *locally Lipschitz-β* at x_0. In the case $n = 0$, i.e. $0 \leq \beta \leq 1$, the inequality becomes

$$|f(x) - f(x_0)| \leq K|x - x_0|^\beta. \tag{66}$$

If inequality (65) holds for all x_0 in an interval I (independent of K), then f is said to be *uniformly Lipschitz-β* on I. The larger the Lipschitz exponent β that can be found to satisfy the above, the greater the regularity of f at x_0 (or on I). For example, $\beta = 0$ implies that f is locally bounded; $\beta > 0$ implies that f is continuous at x_0; $\beta > 1$ implies that f is differentiable at x_0, etc.. Negative Lipschitz exponents $\beta < 0$ may also be defined: The Lipschitz exponent associated with the "Dirac delta function" $\delta(x - x_0)$ (in the sense of distributions) is $\beta = -1$.

Here we consider only one particular result involving wavelet transforms of f. Let $\psi(x)$ be a wavelet function on $\mathbf{R}$. The (continuous) wavelet transform of $f(x)$ on $\mathbf{R}$ at the scale $s > 0$ and position x_0 is defined by

$$Wf(x_0, s) = \int_{-\infty}^{\infty} f(x) s^{-1/2} \psi^* \left(\frac{x - x_0}{s} \right) dx \tag{67}$$

(assuming the integral exists). Now let $\psi(x)$ be a wavelet with n vanishing moments, i.e. $\int_{-\infty}^{\infty} x^k \psi(x) dx = 0$ for $0 \leq k < n$. Suppose that $f(x)$ is uniformly Lipschitz-β, $0 < \beta < n$ on an interval I. Then there exists a constant $A > 0$ such that [23]

$$|Wf(x_0, s)| \leq A s^{\beta + 1/2}, \quad \forall\ x_0 \in \mathbf{R},\ s > 0. \tag{68}$$

The dyadic wavelet expansion coefficients c_{nj} correspond to the discrete scales $s = 2^{-n}$ in Eq. (67). Hence,

$$|c_{nj}| \leq A 2^{-n(\beta + 1/2)}, \quad \forall\ x_0 \in I. \tag{69}$$

The uniform Lipschitz behaviour of f implies a uniform asymptotic decay - more precisely, a geometric decay - of wavelet expansion coefficients across a particular refinement/frequency

level n. Expressions for asymptotic decay also exist for the case of local Lipschitz-β behaviour about a point x_0.

Without loss of generality, we consider the simple fractal-wavelet transform M of Example 1 in Section 2.2. Iteration of M produces a wavelet tree whose coefficients c_{nj} behave as follows:

$$|c_{nj}| \leq A|\alpha|^n, \quad 0 \leq j \leq 2^n - 1, \quad n = 1, 2, \ldots, \tag{70}$$

where $A = |c_{00}|$ and $|\alpha| := \max_i\{|\alpha_i|\}$. From the inequalities (69) and (70), we have the connection

$$|\alpha| = 2^{-(\beta+1/2)}, \qquad \beta = -1/2 - \log_2 |\alpha|. \tag{71}$$

As β increases, implying that f is more regular, $|\alpha|$ decreases. As $\beta \to 0^+$, $|\alpha| \to 1/\sqrt{2}$. (Recall that $|\alpha| < 1/\sqrt{2}$ guarantees that the IFSW operator M is a contraction mapping on $l^2(\mathbf{N})$.)

Analogous results exist for the behaviour of the wavelet transform about isolated *singular* points x_0. In these cases, the wavelet transform, hence the wavelet coefficients c_{nj}, *increase* geometrically. (More complicated relations exist for nonisolated singularities.) The net result, which also applies to the two-dimensional case, is as follows: At "smooth" regions of an image, we expect the fractal-wavelet transform to yield scaling coefficients α_{ij}^{λ} with *small magnitudes*. Conversely, near singularities, i.e. *edges*, we expect the scaling coefficients to have larger magnitudes. This is illustrated by the "scaling contour map" for the Lena image in Figure 13(a). The magnitudes of the scaling coefficients obtained from the IFSW approximation in Figure 8(b), where $(k_1^*, k_2^*) = (5, 6)$ are plotted on a 64×64 grid. The magnitude $\| \alpha_{ij} \|$ of each scaling coefficient triple $(\alpha_{ij}^h, \alpha_{ij}^v, \alpha_{ij}^d)$ for each $1 \leq i, j \leq 64$ was computed simply as:

$$\| \alpha_{ij} \| = [(\alpha_{ij}^h)^2 + (\alpha_{ij}^v)^2 + (\alpha_{ij}^d)^2]^{1/2}. \tag{72}$$

In this way, the horizontal, vertical and diagonal edge contributions have been combined into one "edge index." It is clear that larger values of $|\alpha|$, represented by darker squares, are clustered about the irregular regions of the image, i.e. edges. (By representing the $\lambda = \{h, v, d\}$ coefficients with three separate colours, different edge orientations may be distinguished in the contour map.)

In Figure 13(b) is shown a histogram plot of the α_{ij}^{λ} scaling coefficients. (Here, the h, v, d coefficients are considered separately.) In this case, 90% of the coefficients lie in the interval $[-0.6, 0.6]$. In fact, the distributions obtained from the fractal-wavelet transforms of a number of standard images are virtually identical, exhibiting a highly peaked Laplacian-like structure. (The distribution of wavelet coefficients is also observed to be Laplacian in nature.) Figure 13(b) reveals that much of the Lena image consists of smooth regions. The edges, associated with scaling coefficients with large magnitudes, comprise a small fraction of the image. Nevertheless, it is the edges which characterize an image. This is important when considering quantization schemes for scaling coefficients. (Note that a midriser quantization of the α_{ij}^{λ} assigns a value of zero to scaling coefficients in a neighbourhood of zero. Since a zero value of the scaling coefficient implies that the corresponding child quadtree is zero, the process is in some way analogous to *zerotree* wavelet schemes [32].) It is important to be able to code as much higher-resolution information, e.g. edges, into the fractal-wavelet transform. These ideas will be explored further elsewhere [37].

Given an image (function or measure), the determination of "sizes" of subregions with prescribed irregularity/regularity (as measured by Lipschitz or Hölder exponents) is a subject of *multifractal* analysis [20]. On this note, we draw the reader's attention to some recent

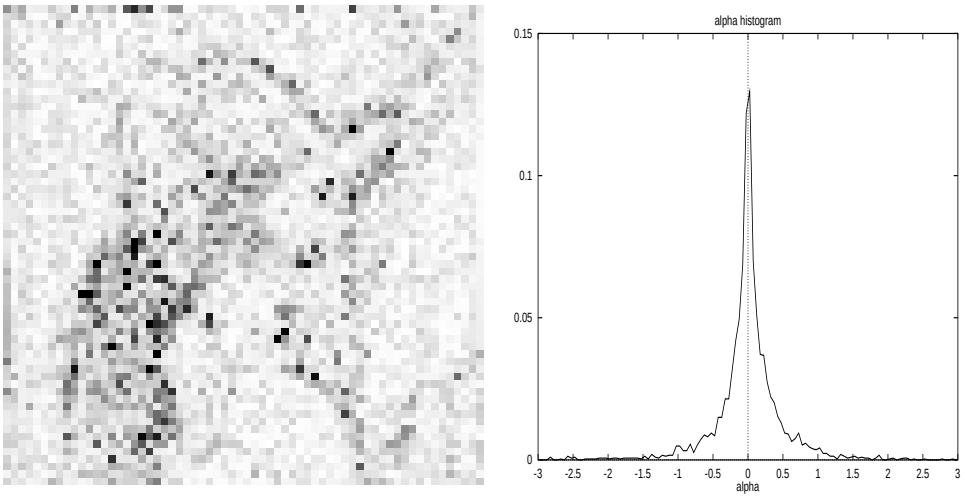

Figure 13. (a) Fractal scaling parameter "contour map." Magnitudes of α_{ij} scaling vectors for $(k_1^*, k_2^*) = (4, 5)$ IFSW approximation of Lena image plotted as a 64×64 array. Higher scaling magnitudes, represented by darker points, are situated at or near edges or irregular regions of the image. (b) Histogram (normalized) of α_{ij}^{λ} values for the (4,5) IFSW approximation of Lena.

and very significant work on the problem of constructing (continuous) fractal interpolation functions with prescribed local Hölder regularity conditions [6, 7]. This has been accomplished by several means, including a *generalized affine IFS* (GIFS) interpolation functions.

6.2 "Fractal Zoom"

Up to this point, the fractal-wavelet transform has been used to extrapolate the wavelet expansion of a image from "zeroth order," i.e. the stored block $\mathbf{B}_{k_2^*}$, to the "complete" expansion of the image, i.e. $\mathbf{B}_9$ for a 512×512 pixel image. However, the fractal-wavelet transform may be iterated even further to produce additional wavelet blocks, e.g. approximations to $\mathbf{B}_{10}$, or 1024×1024 representations of the image, $\mathbf{B}_{11}$, etc.. These correspond to higher resolution approximations of the image. For a fixed pixel size, they permit an approximate "zooming." Figures 14(a) and 14(b) show approximations to $\mathbf{B}_{10}$ and $\mathbf{B}_{11}$ resolutions of the Lena image. In both cases, 512×512 pixel blocks from the centre of each approximation have been plotted.

7 Concluding Remarks

In this paper a generalized class of affine two-dimensional fractal-wavelet transforms has been introduced. The action of these IFS-type operations on wavelet quadtrees induces an action in function space: a *recurrent IFSM with condensation functions* involving dilatation, scaling and mixing of orthogonal components of the image function. Under suitable conditions, the affine IFSW operator is contractive, leading to a fractal approximation method based on the collage theorem. The fixed point wavelet tree $\bar{c}$ of the contractive operator exhibits a kind of "self-tiling": it is expressible as a union of an upper "parent" blocks with scaled copies below them.

The compression methods employed in this study were quite simple. Further investigation is required in a number of areas including: (1) less restrictive parent-child configurations where the refinement can be adaptive, (2) a detailed analysis of searching *vs.* nonsearching

Figure 14. "Fractal zooming" obtained from $(k_1^*, k_2^*) = (5, 6)$ IFSW transforms. (a) Wavelet coefficients extrapolated to $\mathbf{B}_{10}$. (b) Extrapolation to $\mathbf{B}_{11}$.

or partial searching of parent quadtrees, (3) the role of quantization and entropic coding, (4) exploitation of possible correlations between the three sets - h, v, d - of the α_{ij} scaling coefficients. (5) the use of more than one scaling coefficient for a given quadtree collage. From the discussion in Section 5, the IFSW method extrapolates low frequency wavelet coefficients from a knowledge of higher frequency behaviour. The extrapolated coefficients grow or decay geometrically according to the magnitudes of the affine scaling factors α_{ij}^{λ}. From the discussion in Section 5, these scaling factors are intimately related to the local regularity/irregularity properties of the image. As such, the fractal-wavelet transform is, in some way, encoding edge and smoothness information of the image. Perhaps there are even better ways to encode this important information in the IFSW transform. One must keep in mind that the discussion was very simple, being limited to isolated singularities. It remains to analyze thoroughly the connection between wavelet transform scaling results and fractal-wavelet transforms. It may also be helpful to define IFSW which employ nonlinear transformations of wavelet subtrees.

It is also possible to use "fractal zooming" to enhance images where high frequency information may be lacking. The results of some work in this area, along with (3)-(5) above, will be reported elsewhere [37].

In closing we draw the reader's attention to some recent work in which edge information encoded in low order DCT/JPEG coefficients is used to improve the fractal approximation [38]. The use of fractal transforms to enhance JPEG compressed images is also reported.

Acknowledgements

It is a pleasure to thank Prof. B. Forte and Dr. F. Mendivil for many discussions as part of the ongoing "Waterloo Fractal Compression Project" (`http://links.uwaterloo.ca`). I also sincerely thank Dr. J. Lévy Véhel of INRIA, Rocquencourt (France) for some extremely helpful discussions, particularly with regard to multifractals and scaling of wavelet transforms. This research was supported in part by the Natural Sciences and Engineering Council of Canada (NSERC) in the form of individual Operating Grants as well as a Collaborative Projects Grant (with C. Tricot, École Polytechnique, U. de Montréal, J.

Lévy Véhel, INRIA, Rocquencourt, France and B. Forte, Verona, Italy), which are hereby gratefully acknowledged.

References

[1] M.F. Barnsley, *Fractals Everywhere*, Academic Press, New York (1988).

[2] M.F. Barnsley and S. Demko, Iterated function systems and the global construction of fractals, Proc. Roy. Soc. London **A399**, 243-275 (1985).

[3] M.F. Barnsley, S.G. Demko, J. Elton and J.S. Geronimo, Invariant measures for Markov processes arising from Iterated Function Systems with place-dependent probabilities. *Ann. Inst. H. Poincaré*, **24**, 367-394 (1988).

[4] M.F. Barnsley and L.P. Hurd, *Fractal Image Compression*, A.K. Peters, Wellesley, Mass. (1993).

[5] P.M. Centore and E.R. Vrscay, Continuity of attractors and invariant measures for Iterated Function Systems, Canad. Math. Bull. **37**(3), 315-329 (1994).

[6] K. Daoudi, *Généralisations des systèmes de fonctions itérés - Applications au traitement du signal*, Doctor of Mathematics Thesis, Université Paris IX Dauphine (1996).

[7] K. Daoudi, J. Lévy Véhel and Y. Meyer, Construction of continuous functions with prescribed local regularity, to appear in Constr. Approx..

[8] G.M. Davis, Self-Quantized Wavelet Subtrees: A Wavelet-Based Theory for Fractal Image Compression, in *IEEE Data Compression Conference Proceedings*, edited by J. Storer. IEEE Computer Society Press, March 1995.

[9] G.M. Davis, A wavelet-based analysis of fractal image compression, preprint, 1996.

[10] I. Daubechies, *Ten Lectures on Wavelets*, SIAM Press, Philadelphia (1992).

[11] Y. Fisher, editor, *Fractal Image Compression, Theory and Application*, Springer-Verlag, New York (1995).

[12] Y. Fisher, editor, *Fractal Image Encoding and Analysis*, Proceedings of the NATO ASI held in Trondheim, Norway, July 8-17, 1995. Springer-Verlag, New York (1997).

[13] D. Field, Scale-invariance and self-similar 'wavelet' transforms: an analysis of natural scenes and mammalian visual systems.

[14] B. Forte and E.R. Vrscay, Theory of Generalized Fractal Transforms, to appear in *Fractal Image Encoding and Analysis*, edited by Y. Fisher, Springer-Verlag, New York (1997). (Proceedings of the NATO ASI held in Trondheim, Norway, July 8-17, 1995.)

[15] B. Forte and E.R. Vrscay, Inverse Problem Methods for Generalized Fractal Transforms, to appear in *Fractal Image Encoding and Analysis*, ibid..

[16] J. Froment and S. Mallat, Second generation compact image coding with wavelets, in *Wavelets - A Tutorial in Theory and Applications*, C.K. Chui (ed.), pp. 655-677, Academic Press, New York (1992).

[17] J. Hutchinson, Fractals and self-similarity, Indiana Univ. J. Math. **30**, 713-747 (1981).

[18] A. Jacquin, Image coding based on a fractal theory of iterated contractive image transformations, IEEE Trans. Image Proc. **1** 18-30 (1992).

[19] H. Krupnik, D. Malah, and E. Karnin. Fractal Representation of Images via the Discrete Wavelet Transform, *IEEE 18th Convention of Electrical Engineering in Israel, Tel-Aviv*, March 1995.

[20] J. Lévy Véhel, Fractal approaches in signal processing (preprint). Introduction to the multifractal analysis of images (preprint).

[21] N. Lu, *Fractal Imaging*, Academic Press, New York (1997).

[22] S.G. Mallat, A theory for multiresolution signal decomposition: The wavelet representation, *IEEE Trans. PAMI*, **11**, No. 7, 674-693 (1989).

[23] S.G. Mallat, *Wavelet Signal Processing*, preprint (1996).

[24] S. Mallat and W.L. Hwang, Singularity detection and processing with wavelets, IEEE Trans. Infor. Th. **38**, 617-643 (1992).

[25] S. Mallat and S. Zhong, Characterization of signals from multiscale edges, IEEE Trans. PAMI **14**, 710-732 (1992).

[26] F. Mendivil and E.R. Vrscay, Correspondence Between Fractal-Wavelet Transforms and Iterated Function Systems, to be presented at the Third "Fractals in Engineering" Conference, Arcachon, France, 25-27 June 1997.

[27] D.M. Monro, A hybrid fractal transform, Proc. ICASSP 5 (1993), pp. 162-172.

[28] D.M. Monro and F. Dudbridge, Fractal Block Coding of Images, *Electron. Lett.* **28**, 1053-1054 (1992).

[29] D.M. Monro and P.D. Wakefield, Zooming with implicit fractals, Proc. ICIP 1997.

[30] G. Oien and S. Lepsoy, On the benefits of basis orthogonalization in fractal compression, i to appear in *Fractal Image Encoding and Analysis*, edited by Y. Fisher, Springer-Verlag, New York (1997). (Proceedings of the NATO ASI held in Trondheim, Norway, July 8-17, 1995.)

[31] A. Said and W.P. Perlman, A new fast and efficient image codec based on set partitioning in hierarchical trees, IEEE Trans. Circuits and Systems for Video Tech, **6** (1996).

[32] J. Shapiro, Embedded image coding using zerotrees of wavelet coefficients, IEEE Trans. Sig. Proc. **41**, 3445-3462 (1993).

[33] B. Simon, Explicit link between local fractal transform and multiresolution transform, Proceedings of the IEEE Conference on Image Processing, October, 1995.

[34] A. van de Walle, Merging fractal image compression and wavelet transform methods, to appear in *Fractal Image Coding and Analysis*, edited by Y. Fisher, Springer-Verlag, New York (1997); *Relating Fractal Compression to Transform Methods*, Master of Mathematics Thesis, Department of Applied Mathematics, University of Waterloo, 1995.

[35] G. Vines, Orthogonal basis IFS, in *Fractal Image Compression, Theory and Application*, Y. Fisher, editor, Springer-Verlag, New York (1995).

[36] E.R. Vrscay, Mathematical theory of generalized fractal transforms and associated inverse problems, Proceedings of ImageTech 96 Conference on Multimedia Imaging Technology and Applications, Atlanta, GA, March 17-20 (1996).

[37] E.R. Vrscay, Image processing with the fractal-wavelet transform, in preparation (1997).

[38] P.D. Wakefield, D.M. Bethel and D.M. Monro, Hybrid image compression with implicit fractal terms, Proc. ICASSP 1997.

[39] G.G. Walter, *Wavelets and Other Orthogonal Systems With Applications*, CRC Press, Boca Raton, FL (1994).

[40] B. Wandell, *Foundations of Vision*, Sinauer Associates, Sunderland, MA (1995).

[41] M. Wickerhauser, *Adapted Wavelet Analysis from Theory to Software*, A.K. Peters, Wellesley, MA (1995).

Appendix A: Some Generalizations of IFSM

Local IFSM: A significant improvement based on a method introduced in 1989 by A. Jacquin lies in the method of "local IFS" [18, 4]. Rather than attempting to express a function as a union of copies of subsets of *itself*, the local IFSM, or LIFSM, method seeks to express it as a union of copies of *subsets* of itself. In other words, the contractive IFS maps $\mathbf{w}$ map subsets of X into smaller subsets of X. We write these maps as $w_{jk} : I_j \to J_k$, where I_j is the *parent* or *domain block* which is mapped into the (smaller) *child* or *range block* J_k.

Example: Let $X = [0,1]$. Suppose that there are two domain blocks $I_1 = [0, 0.5]$ and $I_2 = [0.5, 1]$ and four range blocks $J_i = [(i-1)/4, i/4]$, $1 \leq i \leq 4$. Thus, the IFS maps w_{jk} will have contraction factors $1/2$. Each range block J_i must have a domain block $I_{j(i)}$, $1 \leq j(i) \leq 2$, which is mapped onto it. Associated with each such IFS map $w_{j(i),i}$ is also a grey level map $\phi_i(t)$ which will modify the function values on $I_{j(i)}$ to produce the function values on J_i, $1 \leq i \leq 4$. Suppose that the indices $j(i)$ and grey level maps ϕ_i for the range blocks J_i are given by

i	$j(i)$	$\phi_i(t)$
1	1	$0.66195t - 0.04843$
2	1	$0.28564t + 0.71847$
3	2	$0.28564t + 0.71847$
4	2	$0.66195t - 0.04843$

(In other words, block I_1 is mapped onto range blocks J_1 and J_2, but with different grey level maps.) An approximation of the attractor of this four-map local IFSM is shown in Figure A1. In fact, the domain-range pairs and grey level maps ϕ_i minimize the collage distance associated with approximating the function $\sin(\pi x)$ on [0,1] with a two domain block/four range block LIFSM. A much superior approximation to the graph of this function is obtained by this method as compared to the usual IFSM method. Roughly speaking, it is easier to "tile" the graph of $\sin(\pi x)$ with parts of itself. For example, the portion of the graph supported on $[0, 1/4]$ is better approximated as a shrunken copy of the graph supported on $[0, 1/2]$ as opposed to a shrunken copy of the entire graph supported on $[0, 1]$.

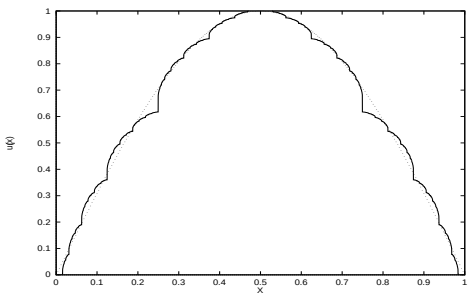

Figure A1: The attractor function $\bar{u}(x)$ of the four-map local IFSM given in the text. It is an approximation to the target function $\sin(\pi x)$ which is also shown.

Place-Dependent IFSM: The grey-level maps have the $\phi_k : \mathbf{R} \times X \to \mathbf{R}$, $1 \leq k \leq N$. Much of the theory developed above for IFSM easily extends to place-dependent IFSM [14].

The fractal components $f_k(x)$ of a function $u \in \mathcal{L}^p(X, \mu)$ will be given by

$$f_k(x) = \begin{cases} \phi_k(u(w_k^{-1}(x)), w_k^{-1}(x)), & x \in w_k(X), \\ 0, & x \notin w_k(X). \end{cases} \tag{73}$$

The operator T associated with an N-map PDIFSM $(\mathbf{w}, \Phi)$ will have the form

$$(Tu)(x) = \sum_{k=1}^{N}{}' \phi_k(u(w_k^{-1}(x)), w_k^{-1}(x)), \tag{74}$$

It is convenient to work with ϕ maps which are only first degree in the grey-level variable t, i.e.

$$\phi(t, s) = \alpha t + \beta + g(s), \quad g : X \to \mathbf{R}, \text{ bounded on } X, \tag{75}$$

$$\phi(t, s) = \alpha(s)t + \beta(s), \quad \alpha, \beta : X \to \mathbf{R}, \text{ bounded on } X. \tag{76}$$

The action of the first set of maps can be considered as a "place-dependent" shift in grey-level value. The second set of maps produce a more direct interaction between position and grey-level value.

Example: The 2-map PDIFSM on [0,1] with IFS maps $w_1(x) = \frac{1}{2}x$, $w_2(x) = \frac{1}{2}x + \frac{1}{2}$ and grey-level maps

$$\phi_1(t, s) = \frac{1}{2}t + \frac{1}{2}, \quad \phi_2(t, s) = \frac{1}{2}t + \frac{1}{2} + \gamma s, \tag{77}$$

where $\gamma \in \mathbf{R}$ may be considered as a "perturbation" parameter for the place-dependent term. When $\gamma = 0$, $\bar{u}(x) = 1$ (a.e.). In Figure A2 are presented histogram approximations of fixed points $\bar{u}$ for two cases, $\gamma = \pm\frac{1}{2}$. The place-dependent term γs produces a gradation or "ramping" of the function over the interval [0,1].

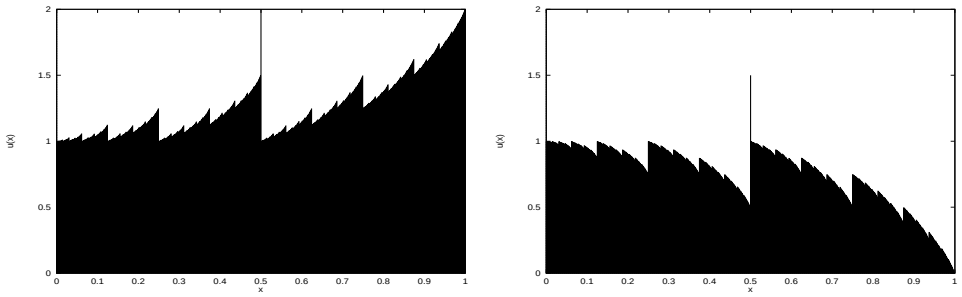

Figure A2: Fixed-point attractor functions $\bar{u}(x)$ of the 2-map PDIFSM in Eq. (72). When $\gamma = 0$, $\bar{u}(x) = 1$ (a.e.). (a) $\gamma = \frac{1}{2}$. (b) $\gamma = -\frac{1}{2}$.

In the two-dimensional case, i.e. $X = [0, 1]$, relevant to image representation, the affine grey-level maps will have the form

$$\phi_k(t, x, y) = \alpha_k t + \beta_k x + \gamma_k y. \tag{78}$$

Appendix B: Periodized Wavelets

In many applications one needs wavelet bases adapted to a compact interval. For this purpose, periodizing the wavelet basis functions is useful. Furthermore, in practical computations, one often deals with finite data sets and periodizing the discrete transform is simple and clean to implement [41].

For a function $f \in L^2(\mathbf{R})$, define the periodized version of f to be

$$f^*(x) = \sum_i f(x - i) \tag{79}$$

where the sum is over all integers i. This process "wraps" the function f around the interval $[0, 1]$ and sums the various contributions.

Let ϕ be a scaling function for an MRA on $\mathbf{R}$ and ψ be the associated "mother" wavelet. Then the periodized wavelets $\psi^*_{ij}(x)$ form an orthonormal basis of $L^2[0, 1]$ and we have a nested MRA structure as in the case of wavelets on $\mathbf{R}$ [10]. Unfortunately, the translation/scaling relations in Eqs. (2) and (7) of Section 2 do not hold for periodized wavelets. For example,

$$\begin{aligned} \psi^*_{1j}(x) &= \sum_k \psi_{1j}(x - k) \\ &= \sum_k \psi(2x - 2k - j) \\ &\neq \psi^*(2x - j). \end{aligned} \tag{80}$$

As a result, the rather simple scaling analysis of Section 2 is not applicable here. The action of an IFSM associated with an IFSW on periodized wavelets is discussed in [26].

Finally, consider the fractal-wavelet transform of Example 1, Section 2, but now applied to coefficient trees for periodized wavelets. In the Haar case, the result is trivially the same as in Figure 1(a) of Section 2. The periodic attractor function $\bar{u}$ for the Coifman-6 periodized wavelets is shown in Figure B1. (Note that the wavelet coefficients c_{ij} for the graphs in Figures 2(a), 2(b) and B1 are identical.)

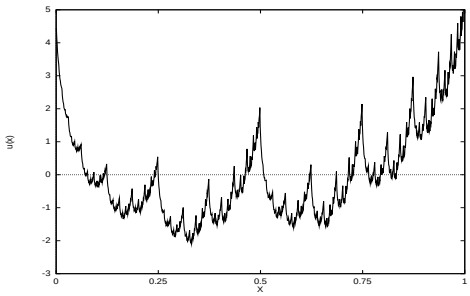

Figure B1. Attractor function $\bar{u}$ for IFSW in Example 1, Section 2.2, using Coifman-6 periodized wavelet functions.